

# The properties of SCUBA cores in the Perseus molecular cloud: the bias of clump-finding algorithms

Emily I. Curtis<sup>1,2\*</sup> and John S. Richer<sup>1,2</sup>

<sup>1</sup>*Astrophysics Group, Cavendish Laboratory, J. J. Thomson Avenue, Cambridge, CB3 0HE*

<sup>2</sup>*Kavli Institute for Cosmology, c/o Institute of Astronomy, University of Cambridge, Madingley Road, Cambridge, CB3 0HA*

Accepted 2009 October 21; Received 2009 October 7; in original form 2009 August 11

## ABSTRACT

We present a new analysis of the properties of star-forming cores in the Perseus molecular cloud, identified in SCUBA 850  $\mu\text{m}$  data originally presented by Hatchell et al. (2005). Our goal is to determine which core properties can be robustly identified and which depend on the extraction technique. Four regions in the cloud are examined: NGC 1333, IC348/HH211, L1448 and L1455. We identify clumps of dust emission using two popular automated algorithms, CLFIND and GAUSSCLUMPS, finding 85 and 122 clumps in total respectively. Using the catalogues of Hatchell et al. (2007), we separate these clumps into starless, Class 0 and Class I cores. Some trends are true for both populations: clumps become increasingly elongated over time; clumps are consistent with constant surface brightness objects (i.e.  $M \propto R^2$ ), with an average brightness  $\approx 4$ –10 times larger than the surrounding molecular cloud; the clump mass distribution (CMD) resembles the stellar initial mass function, with a slope  $\alpha = -2.0 \pm 0.1$  for CLFIND and  $\alpha = -3.15 \pm 0.08$  for GAUSSCLUMPS, which straddle the Salpeter value ( $\alpha = -2.35$ ). The mass at which the slope shallows (similar for both algorithms at  $M \approx 6 M_{\odot}$ ) implies a star-forming efficiency of between 10 and 20 per cent. Other trends reported elsewhere depend critically on the clump-finding technique: we find protostellar clumps are both smaller (for GAUSSCLUMPS) and larger (for CLFIND) than their starless counterparts; the functional form, best-fitting to the CMD, is different for the two algorithms. The GAUSSCLUMPS CMD is best-fitted with a log-normal distribution, whereas a broken power law is best for CLFIND; the reported lack of massive starless cores in previous studies (e.g. Hatchell et al. 2007; Hatchell & Fuller 2008) can be seen in the CLFIND but not the GAUSSCLUMPS data. Our approach, exploiting two extraction techniques, highlights similarities and differences between the clump populations, illustrating the caution that must be exercised when comparing results from different studies and interpreting the properties of samples of continuum cores.

**Key words:** submillimetre – dust: extinction – stars: formation – stars: evolution – ISM: clouds – ISM: individual: Perseus.

## 1 INTRODUCTION

Stars form out of gas in the densest areas of molecular clouds. Early studies of molecular cloud structure (e.g. Blitz & Shu 1980) concluded that a division into discrete clumps of emission was the best description. Within such clumps, star formation occurs inside denser cores (Myers & Benson 1983). A growing consensus now maintains that molecular clouds have a scale-free structure governed by turbulence (e.g. Elmegreen & Falgarone 1996; Stutzki

et al. 1998; Elmegreen & Scalo 2004), with clumps only an arbitrary categorization. We may reconcile these viewpoints to some extent; the clump population has a power-law spectrum of mass implying the overall cloud has a similar distribution (e.g. Williams, Blitz & McKee 2000). Equally, the self-similarity of molecular clouds must break down where gravitational collapse becomes important.

This paper focusses on the decomposition of molecular clouds into *clumps* of emission. The utility of such a description depends on whether the located clumps accurately represent star-forming cores. Clumps are typically located in either dust continuum or spectral-line datasets, which both have their own advan-

\* E-mail: e.curtis@mrao.cam.ac.uk

tages and drawbacks. Continuum observations select high-density cores, which tend to be self-gravitating, but associate more mass to clumps than exists in reality, since objects may be superposed along the line of sight (e.g. Smith, Clark & Bonnell 2008). Clump-finding analyses on spectral-line cubes, with their added velocity dimension, should enable clumps to be more accurately assigned but are subject to larger uncertainties from the details of the radiative transfer than continuum emission. Ultimately, high signal-to-noise ratios are required in both cases for clumps to converge towards the underlying core population (Ballesteros-Paredes & Mac Low 2002).

Nevertheless, many insights into star formation from clump populations remain compelling. Motte, Andre & Neri (1998) first pointed out that the mass distribution of compact continuum clumps (the clump mass distribution; hereafter CMD) is remarkably similar to the initial mass function of stars (IMF). At high masses, the slope is consistent with a Salpeter power law ( $dN/dM \propto M^{-2.35}$ , Salpeter 1955), considerably steeper than the power law for CO clumps ( $dN/dM \propto M^{-1.6}$ , e.g. Blitz 1993). At lower masses, the CMD slope becomes shallower, around the point that samples start to suffer from incompleteness. This suggests that the mass of a star is established at its earliest phases (see also Alves, Lombardi & Lada 2007) and would seem to rule out models where the shape of the IMF is formed later, through e.g. dynamical interactions (Bate & Bonnell 2005). However, the mapping of the CMD on to the IMF is not straightforward and many evolutionary schemes would fit the present data (e.g. Swift & Williams 2008).

Many wide-field surveys are about to or have just begun, which will locate and characterize thousands of star-forming cores from continuum data, e.g. the James Clerk Maxwell Telescope (JCMT) and *Herschel* Gould Belt Surveys (Ward-Thompson et al. 2007b; André & Saraceno 2005). One of the key science drivers for these projects is the measurement of the CMD to high precision at low masses, into the brown-dwarf regime ( $\lesssim 0.08 M_{\odot}$ ). Thus, an examination of different source-finding techniques is particularly timely. Many different methods have been deployed in the literature to locate clumps in molecular-line and continuum data, from identifications by eye to automated algorithms. However, few studies *compare* the sources located with different techniques (a notable exception is Schneider & Brooks 2004). In this paper, we closely compare the populations of continuum clumps found in the Perseus molecular cloud (hereafter simply Perseus) using the two most popular automated algorithms, CLFIND (Williams, de Geus & Blitz 1994) and GAUSSCLUMPS (Stutzki & Güsten 1990), to highlight their differences and biases. We re-examine SCUBA 850  $\mu\text{m}$  data, presented originally by Hatchell et al. (2005), in the four clusters of cores where we have complementary HARP spectral-line data (Curtis, Richer & Buckle 2009), namely: NGC 1333, IC348/HH211 (IC348 for short), L1448 and L1455. Although only investigating a sub-set of the SCUBA data limits our sample size, these are the sources whose kinematics we will investigate subsequently and any CMDs from the spectral-line data will be directly comparable (Curtis & Richer, in prep.). The regions selected still encompass the majority of the SCUBA cores identified by Hatchell et al. (2005, 2007), 58 out of 103; so we can extrapolate any conclusions to the entire cloud population. This work is divided into two principal parts. In Section 3, we identify clumps using the two algorithms before matching them to a catalogue of SCUBA cores, classified as protostellar or starless on the basis of their SEDs by

Hatchell et al. (2007) (hereafter H07). Second, Sections 4 and 5 present an analysis of the physical properties of the cores before we summarize our conclusions in Section 6.

### 1.1 Nomenclature

Many different terminologies have been used to describe the hierarchical structure in molecular clouds; we follow Williams et al. (2000). Within molecular clouds, individual over-densities are termed *clumps*, these are the objects identified by automated algorithms and do not necessarily go on to form stars. Clumps may contain *cores*, which are the direct precursors of individual or multiple stars. Every clump that does not contain an embedded object is referred to as *starless*. Of these starless cores, only a subset, the *prestellar* cores (formerly pre-protostellar cores, Ward-Thompson et al. 1994) will be gravitationally bound and thus go on to form stars.

## 2 OBSERVATIONAL DATA

We extracted fully calibrated and reduced SCUBA 850  $\mu\text{m}$  maps across the four regions in Perseus we observed with HARP from the data presented by Hatchell et al. (2005), where we refer the reader for details of the observations and processing. In short, the data were taken during 20 nights between 1999 and 2003. The sky opacity measured at 225 GHz varied from  $\tau_{225} = 0.039$  to 0.080, with most of the data taken in good conditions ( $\tau_{225} \approx 0.05$ ). The beam size is 14 arcsec (0.017 pc at 250 pc, our assumed distance to Perseus) and the maps are sampled on a 3 arcsec grid. The rms noise level varies across the maps from typical values of  $\sigma_{\text{rms}} = 26 \text{ mJy beam}^{-1}$  in NGC 1333 and IC348 to higher values, 32 and 46  $\text{mJy beam}^{-1}$  in L1448 and L1455. Hereafter, to be consistent with the Hatchell et al. studies and therefore allowing a direct comparison of our source catalogues, we take the noise to be  $\sigma_{\text{rms}} = 35 \text{ mJy beam}^{-1}$ , the typical value for the *entire* cloud.

## 3 THE POPULATION OF DUST CLUMPS

(Sub)millimetre continuum mapping selects young, cold cores (5–20 K) at the earliest stages of star formation. These largely self-gravitating cores are intermediate in properties between CO clumps and infrared young stellar objects (see Ward-Thompson et al. 2007a for a review). The dust’s thermal emission is optically thin nearly everywhere at these wavelengths, accurately tracing density throughout the cloud.

### 3.1 Algorithms

We use CUPID (Berry et al. 2007)<sup>1</sup> to identify clumps of emission in the SCUBA 850  $\mu\text{m}$  maps, exploiting the two most widely used algorithms:

<sup>1</sup> Distributed as part of the Starlink software collection, see <http://starlink.jach.hawaii.edu>.

(i) ‘Clumpfind’ or CLFIND (Williams et al. 1994), which contours the data at evenly-spaced levels, starting close to the peak value. All distinct contiguous areas are considered above each contour level in turn. If an area has no pixels previously assigned to a clump, it is marked as a new clump. Alternatively if there is a pre-existing clump assignment, that clump is extended to the next lowest contour level. When two or more different assignments exist in an area, the pixels are distributed using a friend-of-friends algorithm.

(ii) GAUSSCLUMPS (Stutzki & Güsten 1990), which uses a least-squares fitting procedure to break-down the data into a number of Gaussian-shaped clumps, in a fashion similar to the CLEAN algorithms used in interferometric mapping.

CLFIND is a partitioning method with each pixel only allocated to a single clump, whereas GAUSSCLUMPS permits any number of clumps to overlap at a single spatial position. This means GAUSSCLUMPS is better at handling blended sources, although its output clumps necessarily conform to a strict Gaussian profile as opposed to the arbitrary shapes from CLFIND.

The way each algorithm finds clumps of emission is controlled by a number of tuning parameters. Our overall aim in this paper is to compare the populations of clumps found *independently* by CLFIND and GAUSSCLUMPS. We therefore try to find the same objects with both algorithms, namely clumps larger than the beam size with peaks greater than  $4\sigma_{\text{rms}}$ , but do not try to make the algorithms find exactly the same identifications clump-to-clump. In so doing, we follow the majority of previous studies and select parameters for each algorithm that are considered optimal for rejecting spurious detections. In an alternative approach, one could try to produce clump catalogues which were as similar as possible. However, the standard algorithm outputs we supply are quite different because of the very different way clumps are found with the two algorithms. Given that we can never definitively know the true, underlying clump population, then selecting one algorithm population to make more similar to the other would be completely arbitrary *a priori*. Indeed, it is only through detailed analysis, such as the one presented in this paper, or Monte-Carlo simulations that such a decision regarding algorithm selection could be made.

### 3.1.1 CLFIND

The most important parameters to tune CLFIND’s output are the value of the lowest contour level ( $T_{\text{low}}$ ) and the contour level spacing ( $\Delta T$ ).  $\Delta T$  of  $2\sigma_{\text{rms}}$  is considered optimal for rejecting clumps otherwise fitted to noise spikes (Williams et al. 1994).  $T_{\text{low}}$  essentially sets the clump peak threshold ( $T_{\text{low}} + \Delta T$ ). After some experimentation we settled on the optimum parameters to find plausible clumps:  $\Delta T$  and  $T_{\text{low}}$  both  $2\sigma_{\text{rms}}$ , so clumps must have peaks  $\geq 4\sigma_{\text{rms}}$ . Additionally, the clumps had to be larger than the beam size and contain at least 7 pixels. We find 85 clumps in this manner which are depicted across the four regions in Fig. 1. The full catalogue of CLFIND detections is listed in Tab. A1.

### 3.1.2 GAUSSCLUMPS

For the GAUSSCLUMPS algorithm the most sensitive tuning parameter was the threshold, the minimum value at which the routine would attempt a model fit ( $4\sigma_{\text{rms}}$ ). As for CLFIND, clumps with

**Table 1.** Number of clumps found for the best configuration of both CUPID algorithms alongside the number of sources in H07.

Algorithm\Region	L1455	L1448	IC348	NGC 1333	Total
H07	5	7	17	29	58
CLFIND	7	16	23	39	85
GAUSSCLUMPS	8	25	24	65	122

widths smaller than the beam size (14 arcsec) were rejected. In total, 122 clumps were located in the four regions as shown in Fig. 2. Tab. A2 provides the full the list of GAUSSCLUMPS identifications.

### 3.1.3 Catalogue differences

Although we identify clumps in the same data with the same algorithm, H07 find fewer clumps (the total number of clumps found in this work and H07 is summarized in Tab. 1). H07 use the IDL implementation of CLFIND on the SCUBA maps with an unsharp mask applied to remove structure on spatial scales  $> 2$  arcmin. The most plausible explanation for this discrepancy is the different clump threshold, although there are other differences. In our catalogue, we include all CLFIND detections found with  $T_{\text{low}} = 2\sigma_{\text{rms}}$  and  $\Delta T = 2\sigma_{\text{rms}}$ . This ensures the detections all have peaks  $\geq 4\sigma_{\text{RMS}}$ . However, H07 only select their CLFIND detections (with  $T_{\text{low}} = 3\sigma_{\text{rms}}$  and  $\Delta T = \sigma_{\text{rms}}$ ) that have peaks  $\geq 5\sigma_{\text{rms}}$ . Additionally, they select less bright sources, with peaks  $\geq 3\sigma_{\text{rms}}$  that also have an identification by eye in their original paper (Hatchell et al. 2005) or are Bolocam sources (Enoch et al. 2006).

## 3.2 Distinguishing starless and protostellar clumps

To classify the clumps as starless or protostellar, we looked for an associated source in the identifications of H07. The positional offset from each of our clumps’ peak to the peak of its nearest H07 core in units of the observed clump diameter is plotted in Fig. 3 (cf. similar analysis of Enoch et al. 2008). The diameter along each axis is twice the clump size, where the size is the standard deviation of the pixel coordinates about the centroid, weighted by the pixel values. We associate clumps with a core if they lie within one diameter. For CLFIND, 53 matching clumps (62 per cent of the total) were located within one diameter of the H07 source. All but two of these 53 are within half a diameter. Indeed most of our clumps lie directly on top of the H07 sources so we can confidently classify them. The GAUSSCLUMPS results are similar with 52 clumps (43 per cent) matching to within one diameter. All but four of these lie within half a diameter. Three clumps are paired with two sources, as their emission is sufficiently large to encapsulate two H07 cores. The separation of the H07 cores and Gaussian clumps is significantly larger than the near perfect alignment of the CLFIND clumps. However, the associations are still unambiguous and far from a random distribution.

## 3.3 Dust mass estimates

The mass of a clump,  $M_{850}$ , is proportional to its total 850  $\mu\text{m}$  flux,  $S_{850}$ , provided the emission is optically thin and its only source is thermal emission from the dust:

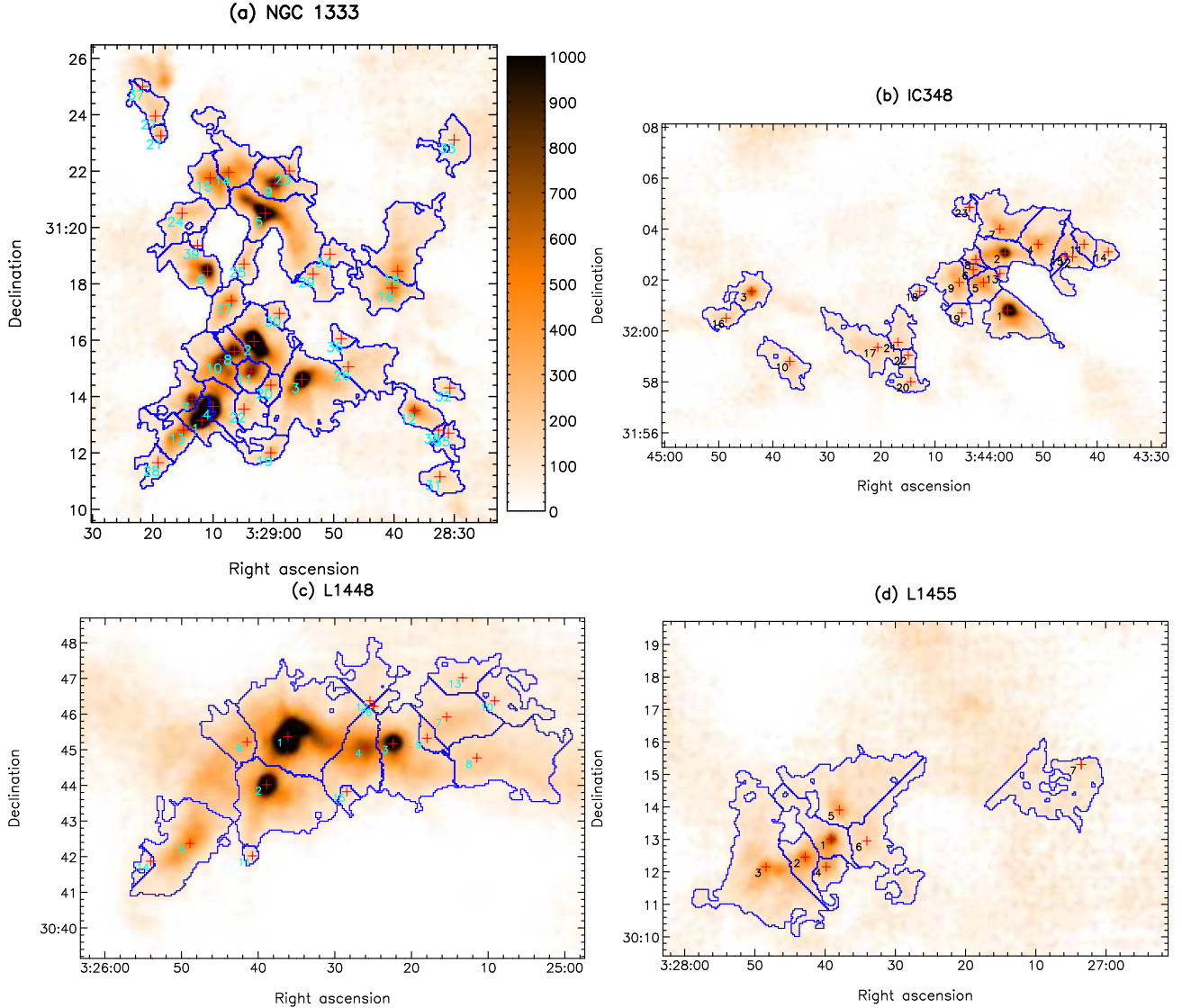


**Figure 1.** Clumps found with CLFIND in (a) NGC 1333, (b) IC348/HH211, (c) L1448 and (d) L1455. The regions selected are where we have complementary HARP data (Curtis et al. 2009). The colour-scale is 850  $\mu\text{m}$  SCUBA flux density from 0 to 1000  $\text{mJy beam}^{-1}$ . The contours show the *boundaries* of the clumps and crosses mark the emission peaks, labelled with the clump number from the catalogue.

$$M_V = \frac{d^2 S_V}{B_V(T_D) \kappa_V}, \quad (1)$$

where  $\kappa_V$  is the dust opacity,  $d$  the distance to the object and  $B_V$  the Planck function at  $T_D$ , the dust temperature. Here the conversion becomes:

$$M_{850} = 0.70 S_{850} \left[ \exp\left(1.4 \left(\frac{12\text{K}}{T_D}\right)\right) - 1 \right] \times \left(\frac{\kappa_{850}}{0.012 \text{cm}^2 \text{g}^{-1}}\right)^{-1} \left(\frac{d}{250 \text{pc}}\right)^2 M_\odot. \quad (2)$$

As discussed in Curtis et al. (2009), we assume a constant distance of 250 pc to the entirety of the Perseus complex. Initially, we adopt  $T_D = 12$  K everywhere. This temperature is consistent with the typical kinetic temperatures ( $T_k \sim 11$  K) derived

by Rosolowsky et al. (2008) from ammonia observations towards 193 dense core candidates in Perseus and dust temperature measurements at 5 arcmin resolution of the whole of the cloud (Schnee et al. 2008). Schnee et al. (2008) find Perseus uniformly cool ( $T_D \sim 12$ – $20$  K) with a median  $T_D = 15$  K. When the sources are separated into classes by age, we assume a slightly higher temperature for those with an internal source of luminosity, i.e. protostars (15 K), over starless cores (10 K). This is consistent with the average isothermal dust temperatures found in protostellar radiative transfer models (Shirley, Evans & Rawlings 2002; Young et al. 2003) and complementary studies (Hatchell & Fuller 2008; Enoch et al. 2008). A final uncertainty in the mass comes from  $\kappa_V$ . We adopt a value,  $\kappa_V = 0.012 \text{cm}^2 \text{g}^{-1}$ , derived from the icy coagulated grain model (number 5) of Ossenkopf & Henning (1994), which is consistent with Hatchell et al. (2005). Kirk, Johnstone &

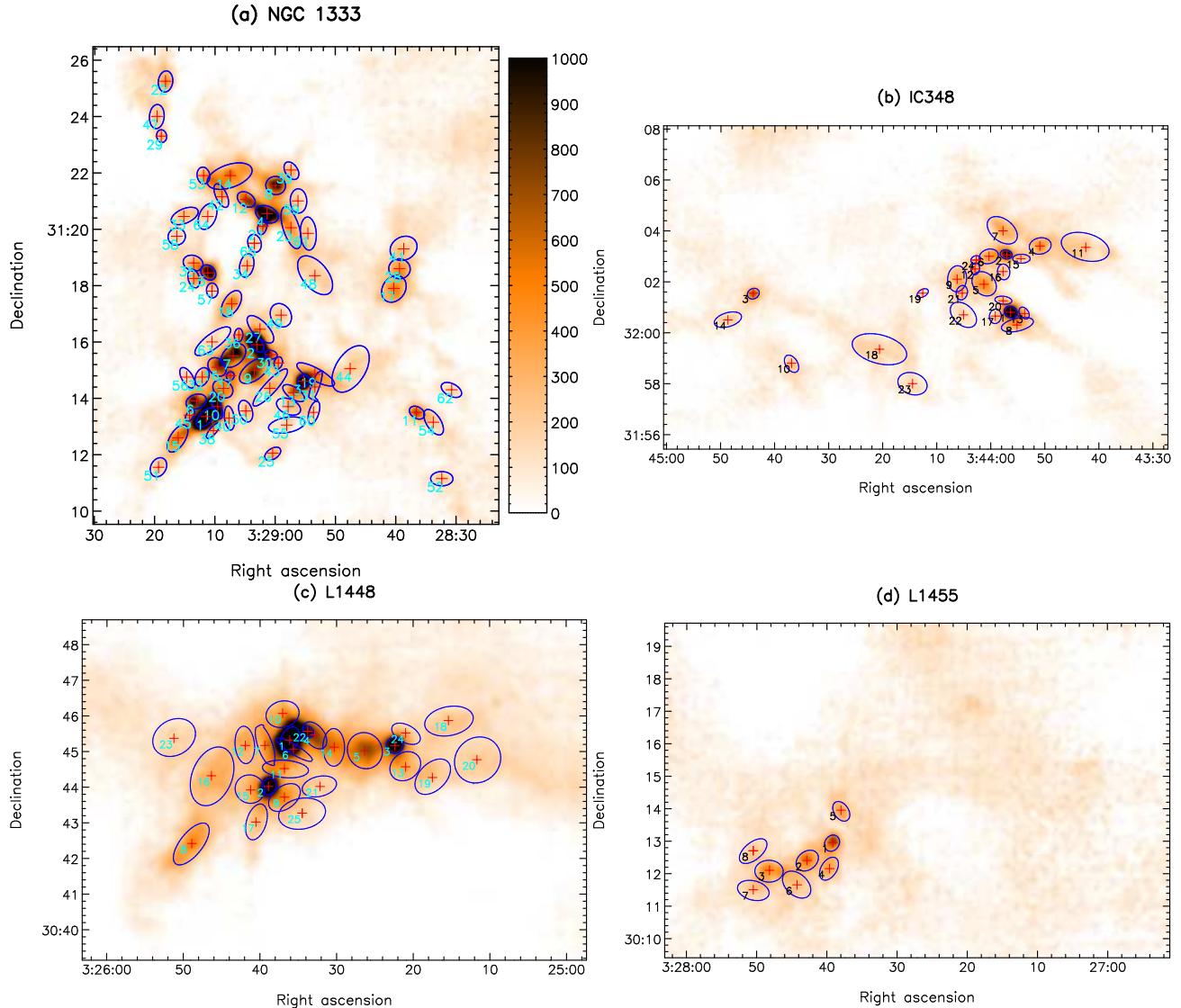


**Figure 2.** Clumps found with GAUSSCLUMPS in (a) NGC 1333, (b) IC348/HH211, (c) L1448 and (d) L1455. The regions selected are where we have complementary HARP data (Curtis et al. 2009). The colour-scale is 850  $\mu\text{m}$  SCUBA flux density from 0 to 1000  $\text{mJy beam}^{-1}$ . The contours show the full-width half-maximum (FWHM) of the Gaussian model fit for each clump with crosses at the emission peak, labelled with the clump number from the catalogue.

Di Francesco (2006), for example, prefer  $0.02 \text{ cm}^2 \text{ g}^{-1}$ , which results in our calculated masses being smaller by a factor of 1.7 for a source of identical flux density.

### 3.4 Completeness

Completeness critically affects any CMD. At low masses, sensitivity limits cause a reduction in the number of clumps found and this could be confused with a turn-over in the mass spectrum. Furthermore, this completeness limit is a function of the clump mass, radius and profile. Massive, extended cores as well as all low-mass cores will be difficult to detect. Assuming constant surface brightness, a clump the size of the beam (radius 7 arcsec) must have at least a mass of  $\sim 0.10 M_{\odot}$  for detection. At the mean radius of the CLFIND clumps (21.4 arcsec, 0.026 pc)  $0.95 M_{\odot}$  is required, whilst

an average sized (17.1 arcsec, 0.021 pc) GAUSSCLUMPS detection necessitates  $M \geq 0.58 M_{\odot}$ . Uniform surface brightness is one of the simplest assumptions we could make for the clump profile. In reality, dust condensations are more centrally concentrated, with profiles well-fitted to Bonnor-Ebert spheres (e.g. Johnstone et al. 2000; Kirk, Ward-Thompson & André 2005). Higher concentrations ensure lower clump masses for a given radius and peak flux, so the uniform surface brightness estimate should be viewed as an upper limit.

## 4 POPULATION CHARACTERISTICS

In this section we explore the physical properties of the populations, summarized in Tabs. 2 and 3. We examine how a core evolves over time by analysing the populations of different core ages, from

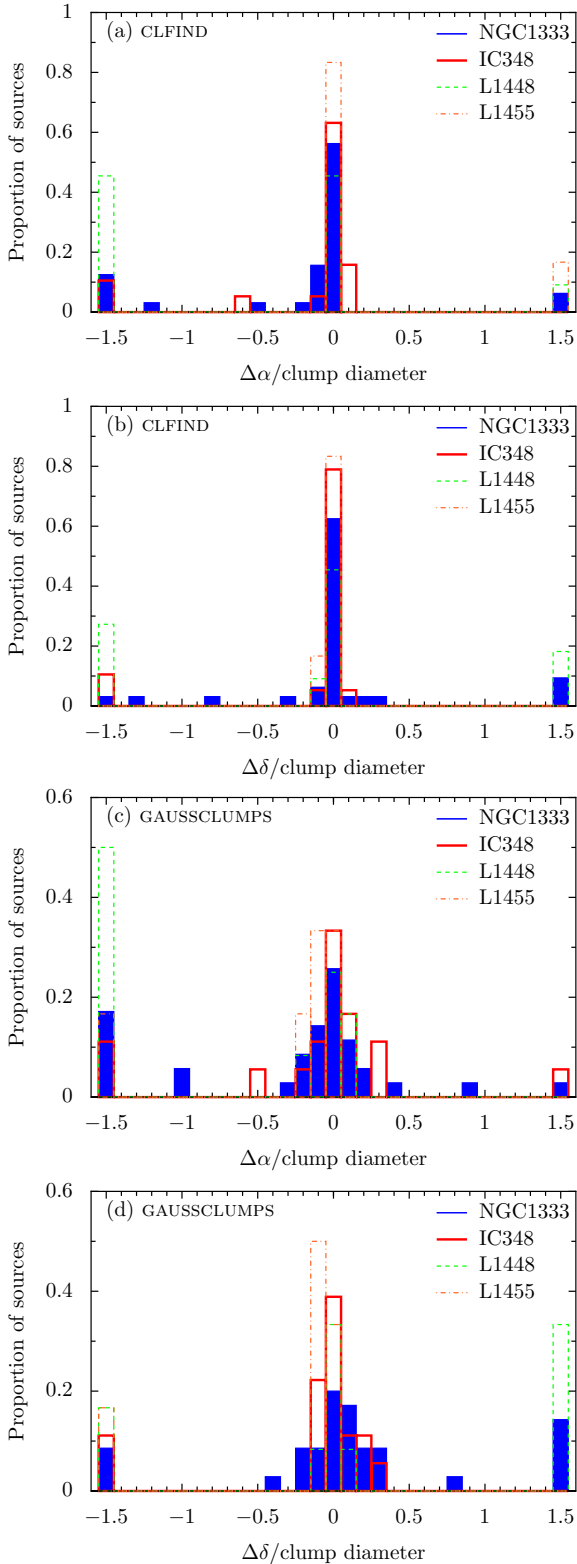


**Figure 3.** Distribution of the positional offsets ( $\Delta\alpha, \Delta\delta$ ) between each clump peak found with CLFIND (top panels, (a) and (b)) or GAUSSCLUMPS (bottom panels, (c) and (d)) and the peak of its nearest H07 core by region. The distances are in units of the measured clump diameter. The alignment is almost perfect for CLFIND and very good for GAUSSCLUMPS.

prestellar to Class I sources, looking for significant differences in the distributions using Kolmogorov-Smirnov (K-S) tests.

Overall, similar numbers of clumps are found for the two algorithms, apart from in L1448 and NGC 1333, where GAUSSCLUMPS finds considerably more. GAUSSCLUMPS fits a strict Gaussian function, which is less flexible in a crowded, high-flux-density area with many clumps probably not following such a profile. Once one model has been subtracted there will still be ample flux in the residuals to continue to fit Gaussians, whereas a method such as CLFIND may distribute this flux to a smaller number of high-mass clumps (e.g. Williams et al. 1994; Smith et al. 2008).

#### 4.1 Size

In Figs. 4 and 5, we plot histograms of the clump deconvolved radius,  $R_{\text{dec}}$ , formed as the geometric mean of the clump major and minor axis sizes (see Section 3.2), each deconvolved with the beam half-width half-maximum (HWHM) size ( $R_{\text{beam}} = 7$  arcsec or 0.0085 pc):

$$\begin{aligned} R_{\text{dec}} &= (R_{\text{dec,maj}} \cdot R_{\text{dec,min}})^{1/2} \\ &= \left( \sqrt{\text{Size}_1^2 - R_{\text{beam}}^2} \cdot \sqrt{\text{Size}_2^2 - R_{\text{beam}}^2} \right)^{1/2} \end{aligned} \quad (3)$$

The CLFIND population has a positively-skewed distribution with mean  $\langle R_{\text{dec}} \rangle = (0.0244 \pm 0.0014)$  pc<sup>2</sup> (see Tab. 2). There are some minor differences region-to-region. IC348 and NGC 1333 have similar distributions to the whole, the former skewed to slightly smaller sizes with  $\langle R_{\text{dec}} \rangle = (0.020 \pm 0.002)$  pc compared to NGC 1333's  $(0.0227 \pm 0.0016)$  pc. L1448 and L1455 have fewer clumps so their distributions are uncertain, but they do appear flatter with means of  $(0.027 \pm 0.003)$  pc and  $(0.041 \pm 0.006)$  pc respectively. K-S tests suggest the NGC 1333 population is significantly different from those in L1448 and L1455 with probabilities of being drawn from the same population of 7 and 2 per cent respectively. Similar results are found for IC348 compared to L1448 and L1455 (5 and 2 per cent).

The trends in the GAUSSCLUMPS data are similar (see Tab. 3). The sizes are smaller than those for CLFIND by  $\sim 0.005$  pc with an overall mean,  $\langle R_{\text{dec}} \rangle = (0.0186 \pm 0.0007)$  pc. The IC348 and NGC 1333 clumps have similar means,  $(0.018 \pm 0.002)$  and  $(0.0176 \pm 0.0009)$  pc respectively. The L1448 population is slightly negatively skewed with the highest average,  $\langle R_{\text{dec}} \rangle = (0.0225 \pm 0.0013)$  pc. K-S tests yield only 1, 3 and 4 per cent likelihoods that the L1448 population is drawn from the same one as NGC 1333, IC348 and L1455 respectively. Clumps in L1455 have changed greatly from their CLFIND distribution; they now have the smallest average,  $\langle R_{\text{dec}} \rangle = (0.017 \pm 0.002)$  pc.

For CLFIND the starless clumps are marginally smaller than the protostellar clumps,  $\langle R_{\text{dec}} \rangle = (0.027 \pm 0.003)$  compared to  $(0.0294 \pm 0.0019)$  pc. The Class 0 and Class I sources have nearly identical means  $((0.0287 \pm 0.0017)$  and  $(0.030 \pm 0.003)$  pc) and similar distributions with the Class 0s narrower. Intriguingly, with GAUSSCLUMPS the opposite trend is clear: on average starless cores are larger than Class 0 sources, which in turn are larger than

<sup>2</sup> All the uncertainties listed throughout this paper are errors on the mean, formed from the sample standard deviations,  $\sigma$ , as  $\sigma/\sqrt{N}$ , where  $N$  is the number in the sample.

**Table 2.** Average clump properties for the CLFIND population. All the errors listed ( $\sigma$ ) are errors on the mean *not* sample deviations.

Population	$R_{\text{dec}}^{\text{a}}$ (pc)	$\sigma_R$ (pc)	AR <sup>b</sup>	$\sigma_{\text{AR}}$	$N(\text{H}_2)^{\text{c}}$ ( $10^{23} \text{ cm}^{-2}$ )	$\sigma_N$ ( $10^{23} \text{ cm}^{-2}$ )	$M$ ( $M_{\odot}$ )	$\sigma_M$ ( $M_{\odot}$ )
All	0.0244	0.0014	1.50	0.07	1.40	0.18	6.4	0.8
NGC 1333	0.0227	0.0016	1.44	0.10	1.7	0.3	6.8	1.2
IC348/HH211	0.020	0.002	1.61	0.17	0.93	0.18	3.6	0.7
L1448	0.027	0.003	1.50	0.15	1.5	0.5	9	3
L1455	0.041	0.006	1.42	0.10	0.93	0.16	8	2
Starless	0.027	0.003	1.46	0.09	1.00	0.15	6.0	1.4
Protostars <sup>d</sup>	0.0294	0.0019	1.42	0.10	2.6	0.4	10.6	1.7
Class 0	0.0287	0.0017	1.37	0.06	3.4	0.5	12	3
Class I	0.030	0.003	1.47	0.19	0.9	0.2	7.6	1.8

<sup>a</sup> Deconvolved radius, see Section 4.1.

<sup>b</sup> Axis ratio, see Section 4.2.

<sup>c</sup> Peak beam-averaged column density, see Section 4.3.

<sup>d</sup> The entire Class 0 and Class I protostellar population.

**Table 3.** Average clump properties for the GAUSSCLUMPS population. All the errors listed ( $\sigma$ ) are errors on the mean *not* sample deviations.

Population	$R_{\text{dec}}^{\text{a}}$ (pc)	$\sigma_R$ (pc)	AR <sup>b</sup>	$\sigma_{\text{AR}}$	$N(\text{H}_2)^{\text{c}}$ ( $10^{23} \text{ cm}^{-2}$ )	$\sigma_N$ ( $10^{23} \text{ cm}^{-2}$ )	$M$ ( $M_{\odot}$ )	$\sigma_M$ ( $M_{\odot}$ )
All	0.0186	0.0007	1.62	0.07	1.11	0.12	3.8	0.3
NGC 1333	0.0176	0.0009	1.68	0.11	1.19	0.18	3.8	0.5
IC348/HH211	0.018	0.002	1.69	0.15	0.85	0.16	3.0	0.5
L1448	0.0225	0.0013	1.50	0.10	1.3	0.3	5.1	0.8
L1455	0.017	0.002	1.25	0.07	0.74	0.11	2.3	0.3
Starless	0.023	0.002	1.48	0.10	0.90	0.09	5.2	0.7
Protostars <sup>d</sup>	0.0182	0.0011	1.43	0.07	2.3	0.3	6.8	0.9
Class 0	0.0190	0.0012	1.40	0.10	2.7	0.3	7.6	1.1
Class I	0.017	0.002	1.49	0.09	0.72	0.15	5.4	1.3

<sup>a</sup> Deconvolved radius, see Section 4.1.

<sup>b</sup> Axis ratio, see Section 4.2.

<sup>c</sup> Peak beam-averaged column density, see Section 4.3.

<sup>d</sup> The entire Class 0 and Class I protostellar population.

Class I sources ( $\langle R_{\text{dec}} \rangle = (0.023 \pm 0.002)$ ,  $(0.0190 \pm 0.0012)$  and  $(0.017 \pm 0.002)$  pc respectively).

What do these results reveal about star-forming cores? In each region we might expect the clump sizes to vary according to the nature of the underlying population (i.e. protostellar or starless) and degree of clustering. Tab. 4 quantifies these effects, through the mean density of sources and the percentage of protostars. For CLFIND the small clumps are in NGC 1333 and IC348 with larger clumps in L1455 and L1448. NGC 1333 is the most clustered environment so we would expect smaller clumps, since any measured size is limited by the distance to the nearest source. IC348 is an exception (low source density with small clumps), but its cores are significantly younger with many more designated starless that dominate the overall size statistics (CLFIND finds starless clumps are smaller than protostars). GAUSSCLUMPS should be better at separating blended sources and indeed the clustering in the regions seems to have little bearing on the calculated sizes. The general trend in the population is for starless cores to be larger than protostars. This is the result reported by the Bolocam team (Enoch et al. 2006, 2008) in their larger Perseus survey at 1.1 mm with a similar

Gaussian fitting technique. Interestingly, they found the two types had similar sizes in Serpens and Ophiuchus.

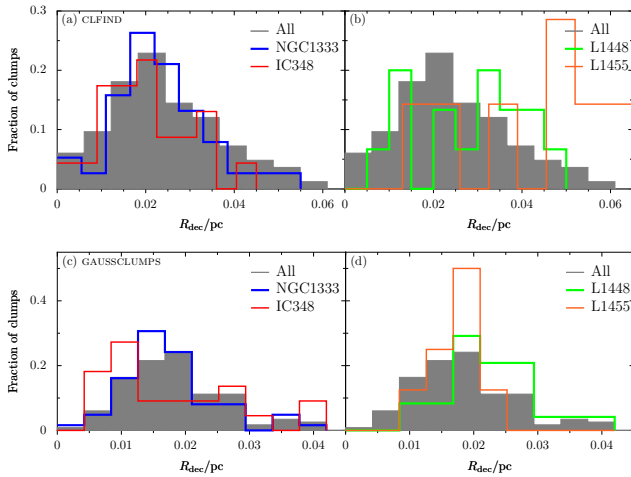
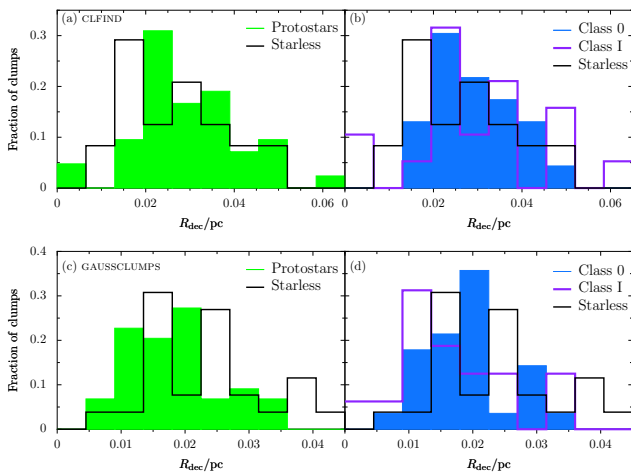
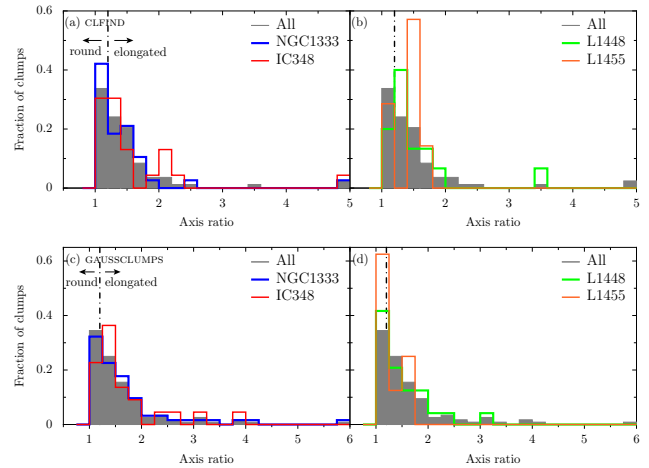
Clearly the type of clump analysis makes a big difference to the interpretation, a K-S test yields only a 1 per cent chance that the two distributions arise from the same population. In general CLFIND finds larger clumps than the tight spread of GAUSSCLUMPS radii. CLFIND produces arbitrary shaped clumps, rather than fitting a strict Gaussian profile. Therefore we might expect more emission at larger distances thus increasing the radii calculated.

## 4.2 Shape

The shapes of star-forming cores provide clues to their formation. Models with cores forming from turbulent flows predict random triaxial shapes with a slight preference for prolateness (Gammie et al. 2003; Li et al. 2004). If strong magnetic fields are present then cores are expected to be oblate (Basu & Ciolek 2004; Ciolek & Basu 2006), which could also be caused by strong rotational motion. Determining the exact 3-dimensional shape of a core from observations is impossible, instead statistical techniques have to

**Table 4.** Clump densities and protostellar fractions. The protostellar fraction is the percentage of Class 0 and we sources out of the total clumps associated with H07 cores.

Region	Area /arcmin <sup>2</sup>	Number of clumps		Mean clump density (arcmin <sup>-2</sup> )		Percentage of protostars in identified sources	
		CLFIND	GAUSSCLUMPS	CLFIND	GAUSSCLUMPS	CLFIND	GAUSSCLUMPS
NGC 1333	190.0	39	65	0.21	0.34	76.9	72.4
IC348	198.6	23	24	0.12	0.12	29.4	31.3
L1448	111.1	16	25	0.14	0.23	80.0	71.4
L1455	127.1	7	8	0.06	0.06	80.0	80.0

**Figure 4.** Distribution of clump radii deconvolved with the beam size,  $R_{dec}$ , broken down by region for the CLFIND (top, (a) and (b)) and GAUSSCLUMPS (bottom, (c) and (d)) populations.**Figure 5.** Distribution of clump radii deconvolved with the beam size,  $R_{dec}$ , for the various core classifications of H07 for the CLFIND (top, (a) and (b)) and GAUSSCLUMPS (bottom, (c) and (d)) populations.**Figure 6.** Distribution of clump axis ratios by broken down by region for the CLFIND (top, (a) and (b)) and GAUSSCLUMPS (bottom, (c) and (d)) populations. The dot-dashed vertical line at a ratio of 1.2 separates clumps Enoch et al. (2006) consider round from those that are elongated.

be applied. Early axisymmetrical work indicated a preference for prolate cores (e.g. Myers et al. 1991) but later studies consistently favour triaxial, preferentially oblate shapes (e.g. Jones, Basu & Dubinski 2001; Goodwin, Ward-Thompson & Whitworth 2002; Tassis 2007; Tassis et al. 2009).

A complete statistical analysis is beyond the scope of this paper, instead we examine the clump ellipticity in 2-dimensions, quantified via the axis ratio. The axis ratio is the ratio of the major to minor clump radii each deconvolved with the beam,  $R_{dec,maj}/R_{dec,min}$ . We plot the distribution of axis ratios in Figs. 6 and 7, whilst summarizing the data in Tabs. 2 and 3. Enoch et al. (2006) performed Monte Carlo simulations of a population of Gaussian sources to see the effects of noise and mapping technique on their Bolocam data in Perseus, which have a similar signal-to-noise ratio as ours. They conclude that a round underlying source can be distorted to reach a maximum axis ratio of 1.2.

Region-to-region the distributions are similar, with K-S tests unable to reject the hypothesis of identical populations to any high level of significance. Most of the distributions have a positive skew with a large proportion of clumps having ratios close to unity. On average, the clumps are slightly elliptical with ratios of  $1.5 \pm 0.07$  for CLFIND and  $1.62 \pm 0.07$  for GAUSSCLUMPS. Starless and protostellar clumps have little difference in their degree of elongation with ratios of  $1.42 \pm 0.10$  and  $1.46 \pm 0.09$  for CLFIND plus



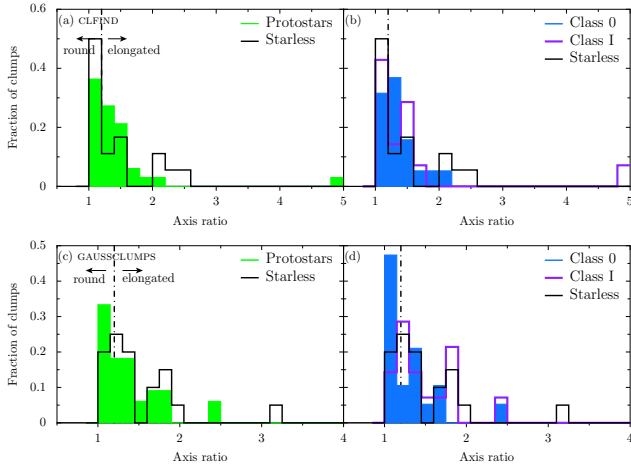


**Figure 7.** Distribution of axis ratios by the source classifications of H07 for the CLFIND (top, (a) and (b)) and GAUSSCLUMPS (bottom, (c) and (d)) populations. The dot-dashed vertical line at a ratio of 1.2 separates clumps Enoch et al. (2006) consider round from those that are elongated.

$1.48 \pm 0.10$  and  $1.43 \pm 0.07$  for GAUSSCLUMPS respectively. Class I sources appear marginally more elongated than Class 0, though the distribution is affected by a few extremely elliptical sources: average ratios of  $1.37 \pm 0.06$  and  $1.47 \pm 0.19$  for Class 0 and I objects with CLFIND alongside  $1.40 \pm 0.10$  and  $1.49 \pm 0.09$  for the same with GAUSSCLUMPS.

Zel'Dovich (1970) and many others since have shown that a dynamically collapsing triaxial ellipsoid will collapse fastest along its shortest axis. Thus as collapse ensues axis ratios increase. This is more or less the picture we see here, with cores becoming slightly more elliptical as they evolve. Surprisingly, Goodwin et al. (2002) found the opposite trend with starless cores more elliptical than protostellar ones in their more sophisticated statistical treatment of the deprojected shape of Jijina, Myers & Adams (1999)'s  $N_2H^+$  cores. This they tentatively propose as evidence of magnetic fields complicating simple gravitational collapse or of an outer protostellar envelope that is not collapsing at all.

### 4.3 Column density

The peak beam-averaged column density of hydrogen,  $N(H_2)$ , depends on the peak 850  $\mu m$  flux,  $F_{850}$ , via:

$$N(H_2) = \frac{F_v}{\Omega_{\text{beam}} \mu m_{H_2} \kappa_v B_v(T_D)} \quad (4)$$

where  $\Omega_{\text{beam}}$  is the solid angle subtended by the beam,  $m_{H_2}$  the mass of a hydrogen molecule and  $\mu = 1.4$  the mean molecular weight per  $H_2$  molecule, assuming 5  $H_2$  molecules for every He. For the values assumed in this paper:

$$N(H_2) = 7.62 \times 10^{22} \left( \frac{F_{850}}{Jy_{\text{beam}^{-1}}} \right) \left[ \exp \left( 1.4 \left( \frac{12 \text{ K}}{T_D} \right) \right) - 1 \right] \times \left( \frac{\kappa_{850}}{0.012 \text{ cm}^2 \text{ g}^{-1}} \right)^{-1} \text{ cm}^{-2}. \quad (5)$$

We take  $T_D$  to be 15 K for protostars, 10 K for starless agglomerations and 12 K otherwise. Figs. 8 and 9 are histograms of the

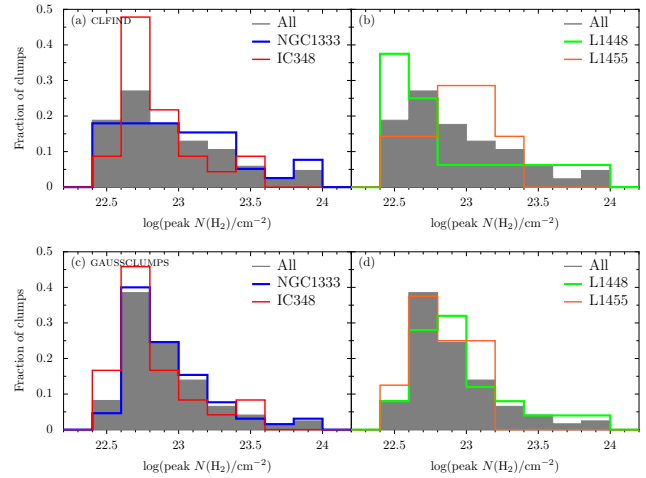


**Figure 8.** Distribution of clump peak beam-averaged column densities for the different regions and overall for the CLFIND (top, (a) and (b)) and GAUSSCLUMPS (bottom, (c) and (d)) populations. The densities were calculated assuming a constant dust temperature of 12 K. All regions exhibit similar behaviour apart from L1455 which has the fewest clumps.

peak clump column density, whereas values for the individual populations are listed in Tabs. 2 and 3. These are necessarily population upper limits since lower density clumps are below our sensitivity threshold. For the first time the CLFIND and GAUSSCLUMPS distributions qualitatively resemble one another, with most clumps falling between  $4$  and  $6.5 \times 10^{22} \text{ cm}^{-2}$ , in the second bin. Their mean log column densities are also close, slightly higher than the most frequent bin at  $(1.40 \pm 0.18) \times 10^{23} \text{ cm}^{-2}$  for CLFIND and  $(1.11 \pm 0.12) \times 10^{23} \text{ cm}^{-2}$  for GAUSSCLUMPS. The distributions' regional variation does not seem to be significant, with only L1455 (with the fewest clumps) showing markedly different behaviour. The breakdown by age is more significant. Similar behaviour is seen for the two algorithms, the protostars and starless cores have similar means,  $(2.6 \pm 0.4) \times 10^{23}$  and  $(1.00 \pm 0.15) \times 10^{23} \text{ cm}^{-2}$  respectively for CLFIND alongside  $(2.3 \pm 0.3) \times 10^{23}$  and  $(0.90 \pm 0.09) \times 10^{23} \text{ cm}^{-2}$  for GAUSSCLUMPS with the protostellar sources having much wider distributions. When the protostars are split into Class 0 and I sources the lower densities are mainly Class I sources (means of  $(9 \pm 2) \times 10^{22}$  and  $(7.2 \pm 1.5) \times 10^{22} \text{ cm}^{-2}$  for CLFIND and GAUSSCLUMPS) with the higher Class 0 sources (means of  $(3.4 \pm 0.5) \times 10^{23}$  and  $(2.7 \pm 0.3) \times 10^{23} \text{ cm}^{-2}$  for CLFIND and GAUSSCLUMPS). From the Class 0/I definition, we have the simple expectation that the more evolved Class I cores have accreted more of their mass on to the central object. So there are lower densities in Class I envelopes, particularly given their smaller or comparable size to Class 0 objects.

### 4.4 Mass versus size relationship

Fig. 10 illustrates the mass-radius relation for the clumps. A least-squares fit to the whole population yields a straight line with a gradient of  $1.7 \pm 0.1$  for CLFIND and  $1.2 \pm 0.2$  for GAUSSCLUMPS. The slope is not well constrained; the constant surface brightness scaling,  $M \propto R^2$ , provides a good fit by eye. The scaling implies a surface brightness,  $\Sigma(H_2) = 1920 M_{\odot} \text{ pc}^{-2}$  and  $\Sigma(H_2) =$

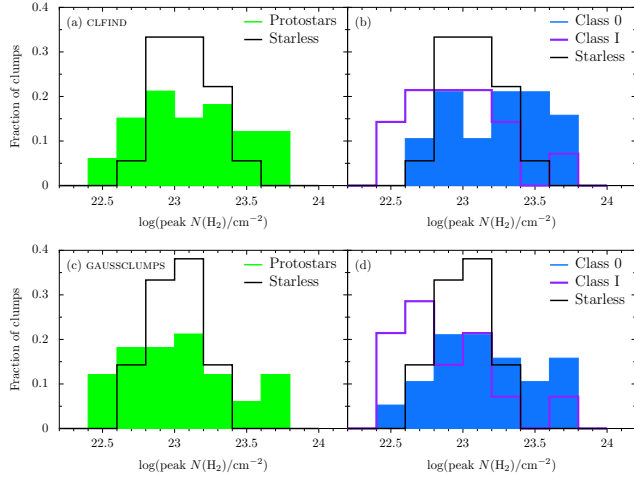


**Figure 9.** Distribution of clump peak beam-averaged column densities for the clumps classified by age in the H07 catalogue for the CLFIND (top, (a) and (b)) and GAUSSCLUMPS (bottom, (c) and (d)) populations. We assume a dust temperature of 10 K and 15 K for the starless and protostellar clumps respectively. Protostars have a similar average density to the starless cores but a wider distribution. The Class 0 sources are roughly the higher density half and Class I is the lower density half of the protostellar distribution.

$2470 M_{\odot} \text{pc}^{-2}$  for the CLFIND and GAUSSCLUMPS sources respectively. These are around ten times higher than the average for molecular clouds as a whole,  $\bar{\Sigma}(\text{H}_2) = 170 M_{\odot} \text{pc}^{-2}$  (Solomon et al. 1987) and four times the largest  $\Sigma$  found by Solomon et al.,  $\sim 500$  (Heyer et al. 2009). This implies there is a large density contrast between the clumps and their surrounding medium.

Enoch et al. (2008) report distinct mass-radius relationships for protostellar and starless cores in Perseus, with the protostars deviating from the tight  $M \propto R^2$  correlation shown by their starless counterparts. They calculate source sizes by fitting an elliptical Gaussian (similar to GAUSSCLUMPS but at previously identified peaks) and masses by integrating the flux within a fixed circular aperture. Our results are slightly different depending on which algorithm is considered. The CLFIND relations are very close to  $M \propto R^2$  for whichever class of object, whereas for GAUSSCLUMPS, the scatter is greater around  $M \propto R^2$ , with a somewhat greater range of masses for a narrower range of sizes in the protostars. This latter observation loosely ties in with the simple suggestion of Enoch et al. (2008) that the present protostellar population in Perseus evolved from prestellar cores which decreased in size and density at constant mass until collapse and protostellar formation. We are only detecting the upper envelope of the mass-radius relationship, the bulk of the cores may exist below the completeness limit. However, the small core numbers in-between the completeness limits for 10 and 15 K cores suggest that we are not missing very many protostellar objects.

In summary, many of the previously reported properties of submillimetre dust clumps depend on the method of identification and care has to be taken to properly account for their biases. For instance, a simple evolutionary model with cores becoming smaller and denser with time would fit the GAUSSCLUMPS radii data with  $R(\text{Starless}) > R(\text{Class 0}) > R(\text{Class I})$ . However, CLFIND data are contradictory:  $R(\text{Starless}) < R(\text{Class 0}) \approx R(\text{Class I})$ . Other pat-

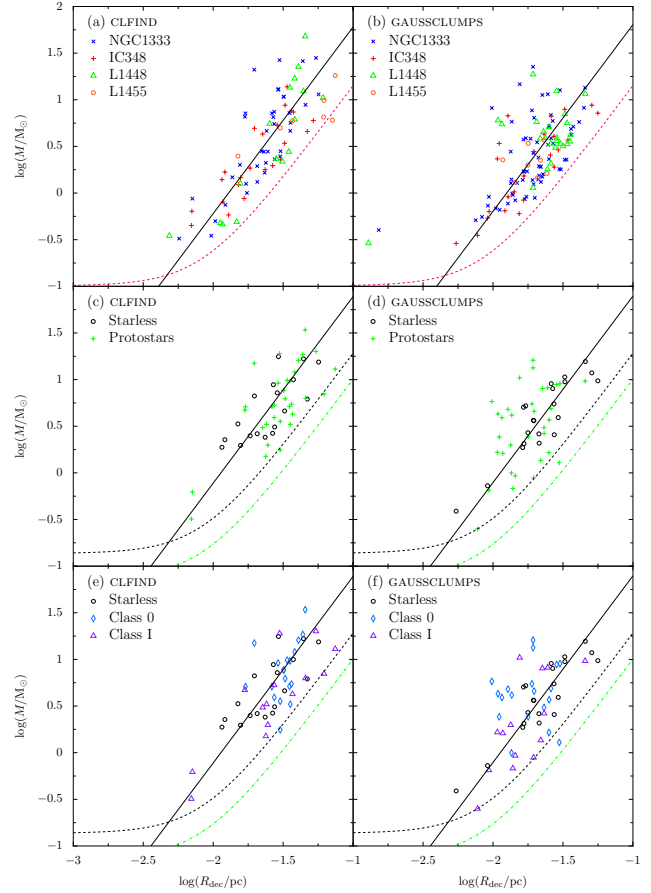


**Figure 10.** Mass versus radius relation for the dust clumps in Perseus. The radius plotted,  $R_{\text{dec}}$ , has been deconvolved with the beam (see Section 4.1). The plots (all on the same scales) are for the CLFIND (left panels, (a), (c) and (e)) and GAUSSCLUMPS (right panels, (b), (d) and (f)) populations, differentiated by region (top panels, (a) and (b)) or by source type from the classifications of H07 (the rest). Lines are drawn at various completeness limits for constant *observed* surface brightness i.e. with  $M \propto R^2$ , where  $R$  in this case refers to the *observed* clump radius (not deconvolved with the beam size). The limits correspond to  $4\sigma_{\text{rms}}$  detections above the noise for 12 K clumps (dashed pink), 10 K starless cores (dashed black) and 15 K protostars (dot-dashed green). Solid black lines mark the best-fitting straight lines of the form  $M \propto R^2$  (i.e. constant surface brightness), either fitted to the whole population (a) and (b) or just the starless clumps (plots (c) and (f)).

terns are more robust – the protostellar and starless populations are similarly elongated and the peak column densities of starless and protostellar clumps are close on average with the Class 0 sources occupying the upper half of the protostars’ distribution and the Class I is the lower. Larson’s Law for constant surface brightness clumps,  $M \propto R^2$ , is obeyed for both algorithms’ clumps with more scatter in the protostellar population of GAUSSCLUMPS.

## 5 THE CLUMP MASS DISTRIBUTION

Every realistic model of star formation must match observations with the fundamental test being whether it reproduces the stellar

IMF. Interpretations of CMDs are complicated by a number of considerations, however appealing a direct one-to-one mapping may seem (see e.g. André, Basu & Inutsuka 2009):

(i) **Form of the distribution.** The differential form of the mass distribution, though easier to interpret, is inaccurate when the number of sources is small ( $\lesssim 100$ ), with a cumulative distribution preferred (Reid & Wilson 2006).

(ii) **Dust properties.** Core masses from continuum measurements are based on uncertain assumptions about the dust itself (i.e. opacity and temperature).

(iii) **Completeness.** Sensitivity limits have the same effect as a real turn-over at lower masses, although in e.g. Nutter & Ward-Thompson (2007), a turn-over significantly higher than the completeness limit is claimed.

(iv) **Nature of the objects.** Many submillimetre cores without a central object will *not* form stars. Molecular-line observations can be useful in discriminating such *unbound* objects from their *bound* brethren (e.g. Curtis & Richer, in prep.).

(v) **Multiplicity.** Some cores will form multiple objects, indeed higher resolution observations often break cores down into smaller constituents. Furthermore, multiple systems can form after the prestellar phase during collapse (e.g. Goodwin et al. 2007).

(vi) **Efficiency.** Typically a constant star-forming efficiency, i.e. how effectively a core turns its mass into stellar material, is invoked to map the CMD on to the IMF. If this efficiency is mass dependent then the mapping can be more complicated (Swift & Williams 2008).

(vii) **Timescales.** Clark, Klessen & Bonnell (2007) note that if core lifetimes depend on mass then the shape of the observed CMD will differ from the true, underlying distribution.

We have already mentioned the striking similarity between the CMD and the stellar IMF and this section is a critical examination of this relationship. To begin, we examine the standard CMD for the SCUBA population, comparing it to previous work and looking at regional and age variations. Finally we will look at some of the distortions that prevent a simple mapping of the CMD on to the IMF.

## 5.1 Form of the mass function

For the initial analysis of the entire region, we mainly use a differential mass function, since its interpretation is more straightforward. For clump numbers fewer than 100, where the arbitrariness of binning becomes important, the cumulative form is preferable (Reid & Wilson 2006). We fit the differential CMD using the following functional forms, the most simple being a single power law:

$$\frac{dN}{dM} = AM^\alpha \quad (6)$$

with  $dN$ , the number of objects in a mass bin of width  $dM$ ,  $\alpha$  the power-law exponent and  $A$  a constant. Frequently, when a turn-over is observed (at break mass,  $M_{\text{break}}$ ), a broken power law is fitted with two components:

$$\frac{dN}{dM} = \begin{cases} A(M_{\text{break}})^{\alpha_{\text{high}} - \alpha_{\text{low}}} M^{\alpha_{\text{low}}} & \text{for } M < M_{\text{break}}, \\ AM^{\alpha_{\text{high}}} & \text{for } M \geq M_{\text{break}} \end{cases} \quad (7)$$

with  $\alpha_{\text{high}}$  and  $\alpha_{\text{low}}$  the power law exponents above and below  $M_{\text{break}}$  respectively. Additionally, we fit a log-normal distribution to the differential CMD:

$$\frac{dN}{dM} = \frac{A}{M\sigma} \exp \left[ -\frac{(\ln M - \mu)^2}{2\sigma^2} \right] \quad (8)$$

where  $\sigma$  is the width,  $\mu$  is related to the characteristic mass and  $A$  a normalization constant.

It is normally assumed that the cumulative form of the CMD is also a power law differing in its exponent from  $\alpha$  by unity:

$$N(> M) = \int_M^\infty \frac{dN}{dM} dM = -\frac{A}{\alpha + 1} M^{\alpha+1} \quad (9)$$

for  $\alpha < -1$ . In reality the sum is not to infinity but some fixed mass,  $M_{\text{max}}$ , resulting from either an actual cut-off or sampling limit. Its shape is then modified:

$$N(> M) = -\frac{A}{\alpha + 1} M^{\alpha+1} + \frac{A}{\alpha + 1} M_{\text{max}}^{\alpha+1} \quad (10)$$

This modification can introduce significant curvature at shallow slopes, which could easily be confused with the need to fit a broken power law.

## 5.2 Differential mass function

The differential mass distribution is presented in Fig. 11. The clumps of both algorithms span a similar range of masses, with those from GAUSSCLUMPS extending to lower masses and cut-off at a smaller maximum mass:  $0.3$  to  $47.8 M_\odot$  with an average,  $\langle M \rangle = 6.4 M_\odot$  for CLFIND and  $0.3$  to  $22.6$  with  $\langle M \rangle = 3.8 M_\odot$  for GAUSSCLUMPS. Maximum-likelihood fits of a power law to the CLFIND data (above the sample average completeness limit as for all our fits), has an exponent,  $\alpha = -1.5 \pm 0.1$ , and reduced chi-squared,  $\tilde{\chi}^2 = 4.0$ . A broken power law provides a better fit ( $\tilde{\chi}^2 = 0.9$ ), with  $\alpha_{\text{low}} = -0.6 \pm 0.1$  for  $M < 6.5 M_\odot$  and  $\alpha_{\text{high}} = -2.0 \pm 0.1$  for  $M \geq 6.5 M_\odot$ . Additionally, a log-normal fit has parameters  $\mu = 1.4 \pm 0.2$  and  $\sigma = 1.2 \pm 0.1$  with  $\tilde{\chi}^2 = 1.9$ . The GAUSSCLUMPS data are similarly poorly fitted by a single power law ( $\alpha = -1.30 \pm 0.08$ ,  $\tilde{\chi}^2 = 3.7$ ) but a broken power law is better ( $\tilde{\chi}^2 = 0.5$ ), with  $\alpha_{\text{low}} = -0.46 \pm 0.07$  for  $M < 5.5 M_\odot$  and  $\alpha_{\text{high}} = -3.15 \pm 0.08$  for  $M \geq 5.5 M_\odot$ . The best-fitting distribution for the increased curvature is log-normal with parameters  $\mu = 1.0 \pm 0.1$  and  $\sigma = 0.97 \pm 0.08$ , resulting in  $\tilde{\chi}^2 = 0.3$ .

Our assumptions can affect the masses by up to a factor of four: e.g. dust temperature, opacity and the distance. Importantly, if these vary *uniformly* for every clump, the *shape* of the distribution would be unchanged, merely translating it along the mass axis, altering the break mass. Non-uniform variations will certainly alter the shape. We will investigate temperature variations between clumps shortly but we completely ignore opacity and temperature changes across individual clumps which would require radiative transfer modelling.

A CMD which closely resembles the IMF implies that the final masses of stars are set at the *prestellar* stage during the core formation process (e.g. Padoan & Nordlund 2002). In other models of star formation e.g. competitive accretion, we would not expect such a direct link with the earliest stages (e.g. Bate & Bonnell 2005). A more realistic scenario might be intermediate between the two with dynamic interactions *and* turbulence playing a role (Klessen & Burkert 2000). The exact shape of the local IMF is still rather uncertain (e.g. Scalo 2005), with estimates of the power law slope from  $\alpha = -2.3$  to  $-2.8$  at masses  $\gtrsim 1 M_\odot$ . For both of our algorithms we find a break in the power law, significantly higher

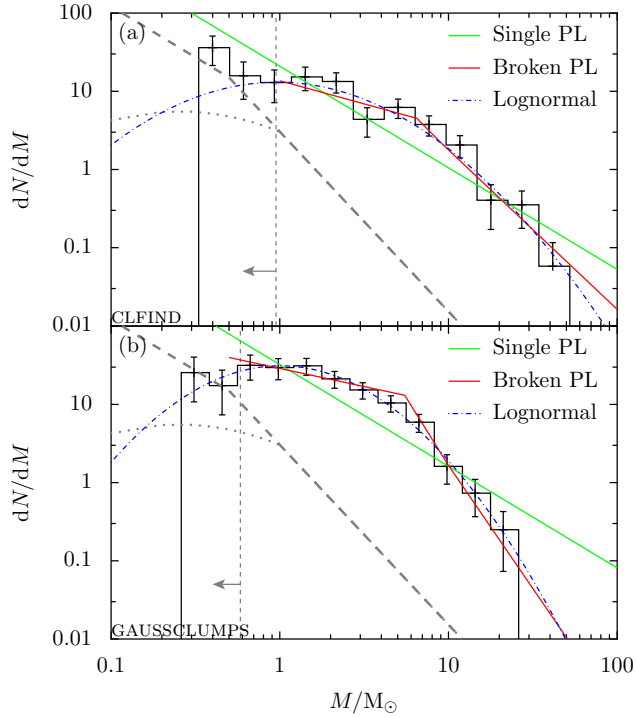


**Figure 11.** Differential mass function of all the submillimetre clumps in Perseus across our four regions. The scales are the same for both plots as is the conversion to mass, with the standard assumptions including a constant clump temperature of 12 K. The error-bars represent Poisson uncertainties. Vertical lines (dashed grey) mark the completeness limits ( $0.95$  and  $0.58 M_{\odot}$  appropriate for CLFIND and GAUSSCLUMPS respectively) calculated for averaged-sized sources of each algorithm population ( $22$  and  $17$  arcsec in turn). Two further lines mark the IMF for single stars (thick dashed grey, Kroupa 2001) and multiple systems (dotted grey, Chabrier 2005). Maximum likelihood fits to the mass function are plotted for various forms: a single power law (solid green), broken power law (solid red) and a log-normal distribution (dot-dashed blue).

than the average sample completeness mass, although it should be stressed the sample is incomplete at every mass. At high masses we find a steeper power law, slightly lower than the Salpeter value for CLFIND and higher for GAUSSCLUMPS. A steeper slope implies a lack of high-mass objects (as is evident from the spread of masses). GAUSSCLUMPS probably misses clump mass at large distances from the clump centre, which can be found by CLFIND as it fits an arbitrary shape. The log-normal CMD fits are somewhat wider than the Chabrier (2005) IMF ( $1.2$  and  $0.97$  compared to  $0.55$ ) and their characteristic masses are a factor of four or so larger ( $1.4$  and  $1.0$  compared to  $0.25 M_{\odot}$ ).

Assuming it is constant, we can estimate the efficiency of star formation,  $\epsilon$ , i.e. how much clump mass is converted into stellar, via the ratios of characteristic masses in the CMD and IMF. We compare the CMD break to the same in the IMF, ( $\sim 0.5 M_{\odot}$ , Kroupa 2001) yielding  $\epsilon = 0.08$  and  $0.09$  for CLFIND and GAUSSCLUMPS respectively. These are considerably smaller than the accepted value of  $0.3$  for embedded clusters (Lada & Lada 2003). Analysing all archived SCUBA data, Nutter & Ward-Thompson (2007) and Simpson, Nutter & Ward-Thompson (2008) find smaller  $M_{\text{break}}$  of  $2.4 M_{\odot}$  in Orion and  $2.0 M_{\odot}$  in L1688 respectively. The

different values suggest the efficiency depends on environment. The break mass can be heavily affected by any assumptions so we must exercise caution when making comparisons between different clouds. For example, the Perseus survey of Enoch et al. (2006) finds the break at  $2.5 M_{\odot}$ , but if we scale our results to match their different assumptions about the dust opacity and clump temperatures, we find our break mass is reduced to  $3.25 M_{\odot}$  for CLFIND and similarly  $2.25 M_{\odot}$  for GAUSSCLUMPS. Correspondingly,  $\epsilon$  increases to  $0.15$  and  $0.22$  respectively and there is less difference between clouds. Nevertheless the lower values of  $\epsilon$  than in clusters are probably because many cores will form multiple stars breaking the one-to-one mapping with the IMF (see Goodwin et al. 2008; Swift & Williams 2008).

A number of further caveats complicate any simple interpretation of the CMD. If higher mass clumps form more stars than lower mass ones, the CMD will be shallower than the IMF arising from it, as we found for CLFIND. Additionally, a clump's current mass may not be representative of the mass available for accretion over its lifetime or the star formation efficiency may vary with mass (see Hatchell & Fuller 2008).

Other groups have measured the CMD in Perseus. The widest survey used Bolocam (Enoch et al. 2006) which we plot alongside our results and the complementary SCUBA analysis of Kirk et al. (2006) in Fig. 12. Enoch et al. (2006) find 122 clumps, using a bespoke algorithm with a more stringent detection limit, a  $5\sigma_{\text{rms}}$  peak above the noise ( $\sigma_{\text{rms}} = 15 \text{ mJy beam}^{-1}$ ) and larger beam ( $31$  arcsec FWHM). Most sources in Perseus lie in five clusters, four of which we analysed, so our comparable numbers are not surprising. Kirk et al. (2006) find considerably fewer sources, only 58, even though they incorporated these data. They used their own data reduction technique, convolved to a degraded map resolution of  $19.9$  arcsec. The resulting maps had higher noise and they used the more stringent  $5\sigma_{\text{rms}}$  peak flux criterion with CLFIND, which probably explains the difference.

Enoch et al. (2006) find a similar spread of masses ( $0.2$  to  $25.6 M_{\odot}$ ), reaching out to lower masses due to their better sensitivity. Kirk et al. (2006) have a narrower range ( $0.2$  to  $9.8 M_{\odot}$ ), the absence of high mass clumps might arise as they have lost sensitivity to low density material with their higher noise and degraded resolution. Both groups adopted different assumptions; to match Enoch et al. (2006) and Kirk et al. (2006), our data would need to be multiplied by  $0.5$  and  $0.9$  respectively. Enoch et al. (2006) find their data is best fitted by a broken power law:  $\alpha_{\text{low}} = -1.3 \pm 0.3$  for  $M < 2.5 M_{\odot}$  and  $\alpha_{\text{high}} = -2.6 \pm 0.3$  for  $M \geq 2.5 M_{\odot}$ . This is slightly steeper than for both of our algorithms at low masses and almost precisely intermediate between CLFIND and GAUSSCLUMPS at high. The Kirk et al. (2006) data are best fitted by a single power law that is quite shallow,  $\alpha = -1.5 \pm 0.2$  but since there is a small number of clumps a cumulative mass distribution is more appropriate.

### 5.3 Regional variations

In Fig. 13, we plot cumulative CMDs for three of our regions in Perseus, L1455 has been excluded because it has a small number of clumps. We use the cumulative form as there are only a small number of cores in each region. The outcomes of maximum-likelihood single and double power law fitting to the CMD with K-S tests to differentiate between the fits are presented in Tabs. 5 and 6. Clumps

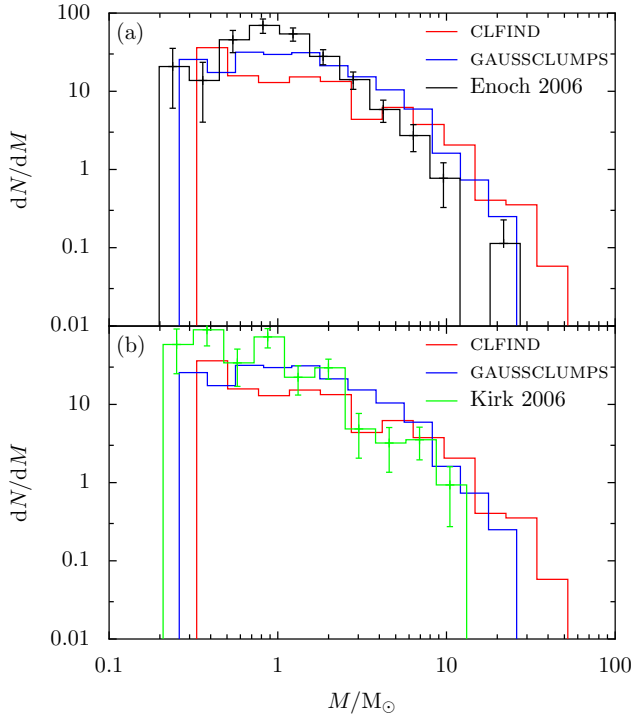


**Figure 12.** Comparison of our differential mass functions, found with CLFIND (red) and GAUSSCLUMPS (blue) to previous work. We plot distributions derived by Enoch et al. (2006) (top panel, black) and Kirk et al. (2006) (bottom panel, green), which correspond closely in shape to our mass functions. Enoch et al. (2006) surveyed  $7.5 \text{ deg}^2$  of Perseus at 1.1 mm with Bolocam on the CSO, whereas Kirk et al. (2006) used the data presented by Hatchell et al. (2005) combined with further independent SCUBA observations to yield a  $3.5 \text{ deg}^2$  survey.

in L1448 are more massive than those in NGC 1333, which are more massive in turn than those in IC348. Returning to the various properties of the regions in Tab. 4, this implies that less clustered regions have more massive clumps (as we may expect from an analogous argument to that employed for the size) and regions that have higher protostellar fractions are more massive. The best-fitting models are typically single power laws with the maximum mass taken properly into account for CLFIND or broken power laws for GAUSSCLUMPS. The high-mass slope appears to be greater for IC348 than NGC 1333 or L1448, although the slope is very sensitive to the exact break mass and fitted model. This is not clear from the fits for GAUSSCLUMPS until the last points are looked at on the plot. Therefore there is a lack of high-mass objects in the IC348, which is likely to be caused by its young population, containing the largest proportion of starless cores. For instance, if starless cores are systematically colder than the assumed temperature (12 K), we would underestimate their masses. Additionally, their masses may be inherently different to protostars as we will explore shortly. The distribution in L1448 varies markedly between the algorithms with the GAUSSCLUMPS slope being significantly steeper than the one for CLFIND. A shallow slope could be explained by its high protostellar fraction, if they are over-estimated in mass by the 12 K assumption or are intrinsically heavier. However, the steep GAUSSCLUMPS slope for L1448 would bring us to the opposite conclusion.

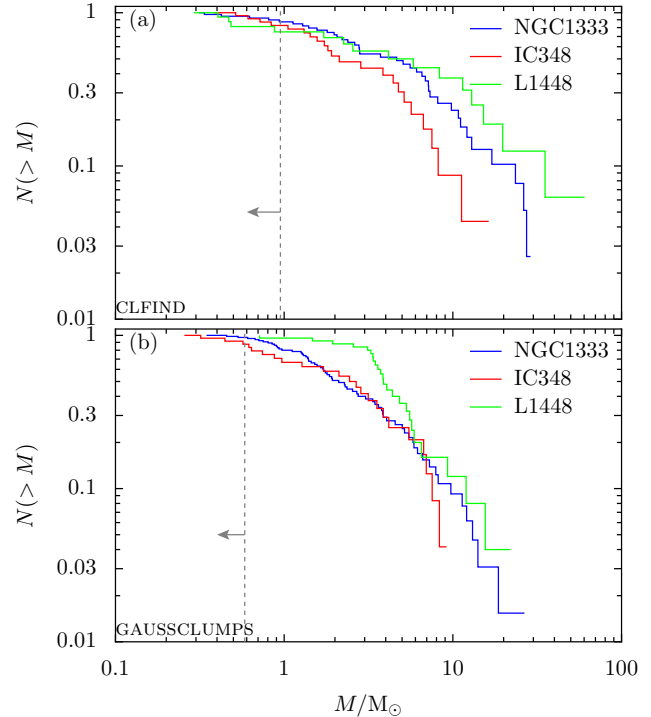


**Figure 13.** Normalized cumulative mass distributions across three of our regions for the CLFIND (top, (a)) and GAUSSCLUMPS (bottom, (b)) populations. The  $4\sigma_{\text{rms}}$  completeness masses for a source of the average sample size are also plotted (dotted grey).

**Table 5.** Best-fitting parameters for various models of the cumulative CMD split up by region. The models that are best-fitting to the data for each region are marked with an asterisk (evaluated using the K-S  $D$  values presented in Tab. 6).

Region \Model	1PL <sup>a</sup> $\alpha$	1PLMM <sup>b</sup> $\alpha$	2PL <sup>c</sup> $\alpha_{\text{low}}$	$\alpha_{\text{high}}$
CLFIND:				
NGC 1333	$-1.58 \pm 0.03$	$-1.089 \pm 0.003^*$	$-1.47 \pm 0.02$	$-2.39 \pm 0.04$
IC348	$-1.79 \pm 0.05$	$-1.15 \pm 0.02^*$	$-1.69 \pm 0.04$	$-2.81 \pm 0.05$
L1448	$-1.46 \pm 0.06^*$	no fit	$-1.32 \pm 0.01$	$-2.39 \pm 0.06$
GAUSSCLUMPS:				
NGC 1333	$-1.68 \pm 0.02$	$-1.43 \pm 0.04$	$-1.60 \pm 0.02$	$-2.55 \pm 0.04^*$
IC348	$-1.56 \pm 0.08$	$-1.0069 \pm 0.0003$	$-1.41 \pm 0.04$	$-2.43 \pm 0.10^*$
L1448	$-1.72 \pm 0.07$	$-1.23 \pm 0.02$	$-1.13 \pm 0.01^*$	$-2.89 \pm 0.04$

<sup>a</sup> Single power law fit (1PL), as in Eq. 9 ( $\alpha$  everywhere corresponds to the gradient of an equivalent differential CMD).

<sup>b</sup> Single power law fit taking into account the finite upper limit of integration (i.e. maximum mass, 1PLMM), as in Eq. 10.

<sup>c</sup> Broken power law fit (2PL).

#### 5.4 Variations by source age

An examination of how the CMD varies with source age can lead to crucial insights into the star formation process. In a trivial mapping on to the IMF, with a constant star-forming efficiency, the shape at the *prestellar* phase may distinguish between models where the mass is set by: (i) the initial fragmentation on to cores, (ii) competitive accretion or (iii) protostellar mechanisms i.e. outflows.

In Fig. 14, we plot the cumulative CMD for protostars and

**Table 6.** K-S  $D$  values for the various fits of the cumulative CMD by region. For the different model names see Tab. 5. An asterisk marks the best-fitting model for each region.

Region & algorithm \ Model	1PL	1PLMM	2PL
NGC 1333, CLFIND	0.13	0.06*	0.17
IC348, CLFIND	0.09	0.06*	0.12
L1448, CLFIND	0.09*	–	0.18
NGC 1333, GAUSSCLUMPS	0.13	0.09	0.08*
IC348, GAUSSCLUMPS	0.33	0.12	0.07*
L1448, GAUSSCLUMPS	0.26	0.20*	0.34

**Table 7.** Best-fitting parameters for various models of the cumulative CMD split up by the source identifications from H07. For the different model names see Tab. 5. The models that are best-fitting to the data for each source population are marked with an asterisk (evaluated using the K-S  $D$  values presented in Tab. 8).

Region \ Model	1PL $\alpha$	1PLMM $\alpha$	2PL $\alpha_{low}$ $\alpha_{high}$	
CLFIND:				
Starless	$-1.69 \pm 0.04$	$-0.62 \pm 0.04^*$	$-1.57 \pm 0.04$	$-5.17 \pm 0.07$
Protostars	$-1.65 \pm 0.04$	$-1.19 \pm 0.01^*$	$-1.53 \pm 0.05$	$-2.71 \pm 0.05$
GAUSSCLUMPS:				
Starless	$-1.52 \pm 0.04$	$-0.68 \pm 0.05^*$	$-1.32 \pm 0.05$	$-2.38 \pm 0.04$
Protostars	$-1.59 \pm 0.04$	$-0.69 \pm 0.04^*$	$-1.48 \pm 0.05$	$-3.71 \pm 0.04$

starless cores with Fig. 15 further breaking the protostars into Class 0 and Is. The masses have been calculated in the usual way assuming isothermal dust temperatures of 10 K for starless and 15 K for protostellar cores. As in Section 5.3, we fit models to the starless and protostellar cumulative CMDs (see Tabs. 7 and 8). For CLFIND, the protostellar CMD is wider, extending to higher and lower masses than the starless equivalent. The situation for GAUSSCLUMPS is more complicated, with the protostellar distribution offset to lower masses than the starless one. When the protostars are further divided, the Class 0 sources have a flatter distribution, containing all the high mass objects, than the Class I or starless distributions with CLFIND. The starless clumps are at lowest masses with the Class Is in the middle. The same holds for the GAUSSCLUMPS decomposition, except the Class I population extends to lowest masses and the starless population out to the highest.

This is the part of the picture described in H07 and Hatchell & Fuller (2008). For the same data analysed in a similar fashion with CLFIND, they find comparable results: Class 0 sources are more massive than Class Is and there is an excess of Class 0 protostars at high masses relative to starless cores – there is a lack of massive

**Table 8.** K-S  $D$  values for the various fits of the cumulative CMD split up by source identifications from H07. For the different model names see Tab. 5. An asterisk marks the best-fitting model for each category.

Region & algorithm \ Model	1PL	1PLMM	2PL
Starless, CLFIND	0.14	0.10*	0.19
Protostars, CLFIND	0.35	0.16*	0.18
Starless, GAUSSCLUMPS	0.23	0.06*	0.09
Protostars, GAUSSCLUMPS	0.15	0.06*	0.11

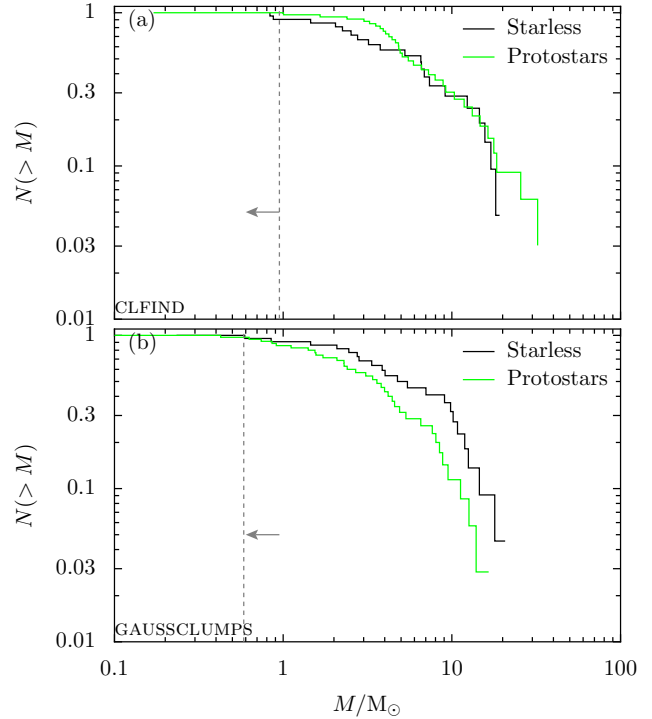


**Figure 14.** Normalized cumulative mass distributions for protostars (green) and starless cores (black) as designated by H07 for the CLFIND (top, (a)) and GAUSSCLUMPS (bottom, (b)) populations. The  $4\sigma_{rms}$  completeness masses for a source of the average sample size are also shown (dotted grey). The masses were calculated assuming a dust temperature of 10 K for the starless and 15 K for the protostellar sources.

starless cores. It is reassuring that the Class 0 sources are more massive than Class Is. The original definition proposed sources to be: Class 0 if the ratio of envelope to central object mass,  $M_{env}/M_*$  > 1 and Class I if  $M_{env}/M_* < 1$  (André, Ward-Thompson & Barsony 1993).

Our results are somewhat inconclusive. Single power law fits to the distributions derived by the two algorithms yield similar slopes for protostellar and starless sources. A power law fit, including the maximum mass term (Eq. 10), has a similar slope for both source types with GAUSSCLUMPS and a shallower slope for the starless cores with CLFIND. This results because the maximum protostellar mass is considerably greater than the starless one, so the necessary curvature is already present and the slope can be shallower. A broken power law, however, has a steeper slope for starless over protostellar cores at the high mass end for CLFIND and the reverse for GAUSSCLUMPS.

All-in-all, the GAUSSCLUMPS distributions are very similar to one another. The Class I population is less massive than the Class 0 and starless populations on average, which is again not surprising given their definition. We expect more evolved sources to have accreted more mass and thereby have less massive dust envelopes. The CLFIND data support the view that the most massive objects are Class 0 protostars and there is a paucity of massive starless cores. This could be explained by dust temperature variations or a mass-dependent evolution of the clumps, with massive prestellar clumps evolving rapidly into protostars, hence not as many are

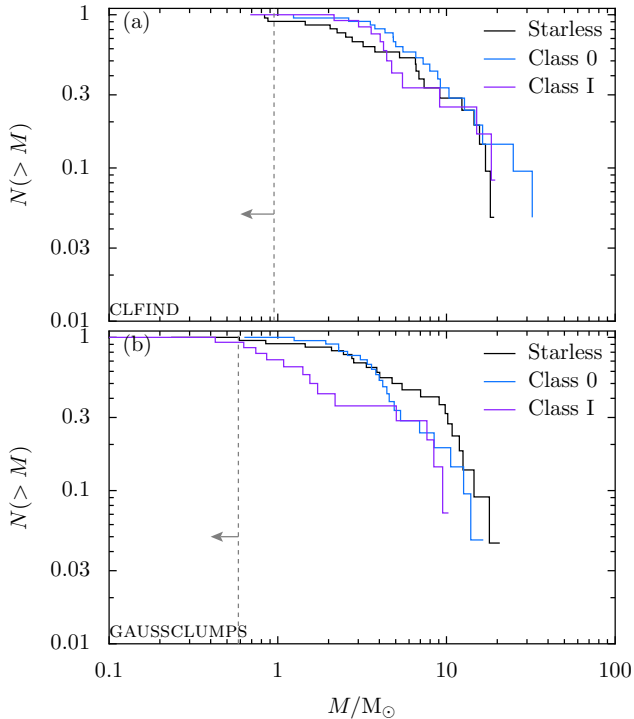


**Figure 15.** Normalized cumulative mass distributions for starless cores (black), Class 0 (blue) and Class I (purple) protostars as designated by H07 for the CLFIND (top, (a)) and GAUSSCLUMPS (bottom, (b)) populations. The  $4\sigma_{\text{rms}}$  completeness masses for a source of the average sample size are also shown (dotted grey). The masses were calculated assuming a dust temperature of 10 K for the starless and 15 K for the Class 0/I sources.

detected (see Hatchell & Fuller 2008). However, if starless cores are not gravitationally bound, then they might not go on to form stars, so placing them in such an evolutionary sequence would be misleading. We examine their dynamic stability in a forthcoming paper (Curtis & Richer, in prep.).

### 5.5 Effect of varying clump dust temperatures

If the dust temperature varies between clumps then the shape of the mass distribution will change. Recently, Rosolowsky et al. (2008) published  $\text{NH}_3$  kinetic temperatures,  $T_k$ , towards 193 positions in Perseus using a beam size of 31 arcsec. If the gas and dust are well-coupled, typically occurring at high densities, we would expect  $T_D \sim T_k$ . Of these atlas positions, 50 coincide with our CLFIND identifications (59 per cent of the clumps,  $\bar{T}_k = (12.9 \pm 0.3)$  K) and 49 with GAUSSCLUMPS sources (40 per cent,  $\bar{T}_k = (12.6 \pm 0.3)$  K). In Fig. 16, we plot the mass distributions for the two algorithms using a varying dust temperature equal to  $T_k$  where it was coincident and 12 K where not. The distribution only changes marginally, indeed Enoch et al. (2008) found the same for a similar analysis on the Bolocam data – the deviation from a power law actually *decreased*. This is not surprising since the average temperature of the clumps is very similar to our assumed dust temperature and their spread is small.

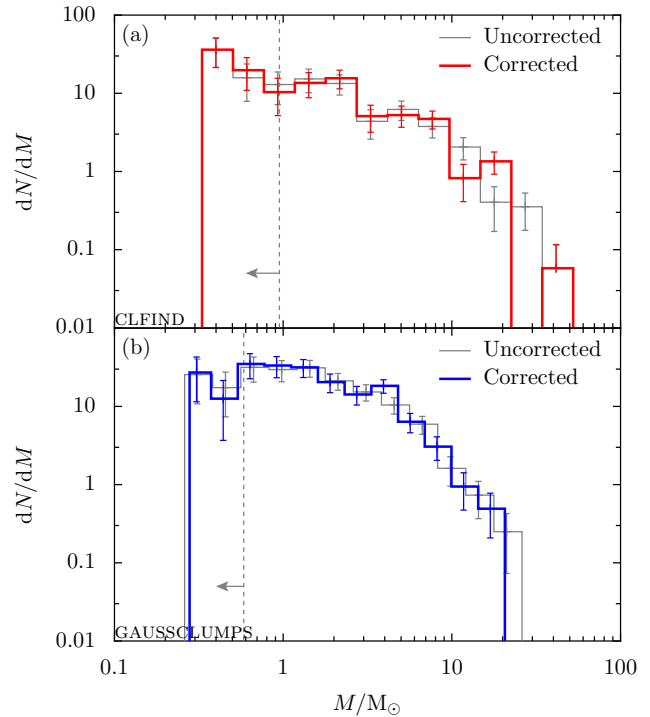


**Figure 16.** Effect of varying clump temperatures on the mass distribution. The original constant-temperature distributions (grey) have been overlaid with ones calculated using  $\text{NH}_3$  kinetic temperatures from the atlas of Rosolowsky et al. (2008) for the CLFIND (top, (a), red) and GAUSSCLUMPS (bottom, (b), blue) populations. The bars are standard Poisson errors on the bins and the  $4\sigma_{\text{rms}}$  completeness masses for a source of average size are also shown (dashed grey).

### 5.6 Effect of clump lifetimes

The observed mass distribution will not be representative of the true distribution if the lifetime of the cores is mass dependent, as we are more likely to detect long-lived cores than short-lived ones. André et al. (2007) suggest a *weighted* mass function, with each core weighted according to the inverse of its free-fall timescale ( $\langle t_{\text{ff}} \rangle / t_{\text{ff}}$ , with  $\langle t_{\text{ff}} \rangle$  the average core free-fall time). Applying such weighting to the cores in Ophiuchus from Motte et al. (1998), they find the break in the power law disappears and a single Salpeter-like power law is the best-fitting. In this section we attempt a similar weighting for our clumps. The free-fall timescale of a homogeneous sphere is:

$$t_{\text{ff}} = \left( \frac{3\pi}{32G\rho} \right)^{1/2} = \left( \frac{\pi^2 R_{\text{dec}}^3}{8GM_{850}} \right)^{1/2} \quad (11)$$

with  $\rho$ , the density in the clump, which we estimate from previously derived quantities as shown. We find free-fall timescales approximately in the range  $10^4$  to  $10^5$  yrs. The resultant weighted distribution is shown in Fig. 17. There is no apparent reduction in the flattening of the distribution at low masses. The reasons for this may be twofold. First, our estimates of the free-fall timescale may be in error. Other groups estimate densities using the mass and radius inside a fixed aperture, whereas our radii are influenced by the whole of the clump. This will tend to reduce the average density of large radius clumps, i.e. large mass clumps, thereby increasing

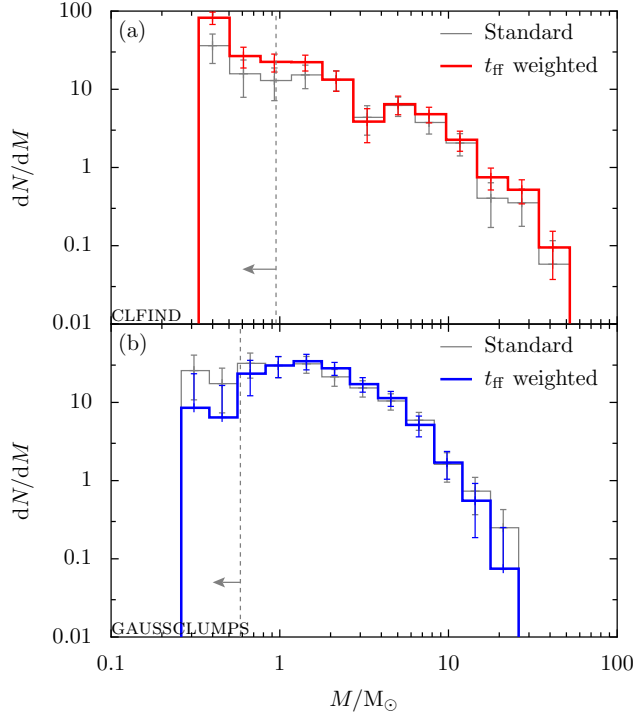


**Figure 17.** Differential mass distribution weighted by the inverse of the clump free-fall timescale,  $\langle t_{\text{ff}} \rangle / t_{\text{ff}}$ , with the original distributions in grey for the CLFIND (top, (a), red) and GAUSSCLUMPS (bottom, (b), blue) populations. The bars are standard Poisson errors on the bins and the  $4\sigma_{\text{rms}}$  completeness masses for a source of average size are also shown (dashed grey).

their free-fall timescales and reducing their corresponding weight in the new distribution. This steepens the mass distribution at large masses and should therefore not affect the presence of a break. Second, there is, as other groups have noted, no relationship between mass and  $t_{\text{ff}}$ . If the break in the CMD is related to differential clump lifetimes then  $t_{\text{ff}}$  should in some way be related to the mass.

## 6 SUMMARY

This paper detailed a new analysis of SCUBA 850  $\mu\text{m}$  data towards NGC 1333, IC348/HH211, L1448 and L1455 in the Perseus molecular cloud. We used two clump-finding algorithms, CLFIND and GAUSSCLUMPS, to decompose the dust column density into clumps of emission. CLFIND located 85 clumps in total, whilst GAUSSCLUMPS found 122. Once identified we divided the clumps into protostellar (Class 0 and I) and starless sources by pairing them with classifications in the catalogues of H07.

This approach highlights trends in the clump properties that are highly or weakly dependent on the clump-finding algorithm. Conclusions which hold regardless of the technique include:

- **Shapes.** Cores are slightly elongated with a tendency to become more elliptical over time as expected from collapse models.
- **Peak column densities.** Protostars and starless cores have similar average peak column densities. The upper half of the protostellar distribution arises from Class 0 protostars and the lower

from Class I. This is expected from the class definitions and supports the classifications of H07. Unsurprisingly, the masses of Class 0 clumps are also larger than Class I.

- **Mass versus size.** Clumps are consistent with the  $M \propto R^2$  relation, having average surface brightnesses some 4-10 times larger than typical giant molecular clouds.
- **CMD.** The clump mass distribution resembles the IMF. The break mass is significantly higher than the average completeness mass and implies a star-forming efficiency of  $\sim 10$ – $20$  per cent, probably reduced relative to embedded clusters due to multiplicity.
- **Regional variations.** The mass of clumps in each region follows:  $M_{\text{clump}}(\text{L1448}) > M_{\text{clump}}(\text{NGC 1333}) > M_{\text{clump}}(\text{IC348})$ . The high-mass slope of the CMD is steeper for IC348 than L1448 with NGC 1333 intermediate.
- **CMD temperature and lifetime dependence.** Using individual temperatures for each clump or weighting according to their free-fall timescale does not change the shape of the CMD.

Other inferences are dependent on the clump identification procedure:

- **Sizes.** Protostars are either larger or smaller than prestellar cores with CLFIND or GAUSSCLUMPS respectively.
- **Functional form of the CMD.** A log-normal CMD is best-fitting to the GAUSSCLUMPS data whereas a broken power law is best for CLFIND. In any case a broken-power-law fit has different slopes for each algorithm, with the GAUSSCLUMPS high-mass slope steeper at  $\alpha = -3.15 \pm 0.08$  than  $\alpha = -2.0 \pm 0.1$  for CLFIND.
- **A lack of massive starless cores?** A shortage of high-mass starless clumps relative to protostars was definitely present in the CLFIND data (see also H07; Hatchell & Fuller 2008). The same was not clear in the GAUSSCLUMPS data, where the overall spread in masses is smaller and the starless cores have larger sizes.

GAUSSCLUMPS can only fit a strict shape so will not allocate flux to a clump at large distances from the peak unlike CLFIND. Therefore the corresponding GAUSSCLUMPS sizes are smaller. The clumps sizes in clustered regions such as NGC 1333 are smaller, as expected, for CLFIND but not any different for GAUSSCLUMPS, which is better at dealing with blended sources. The clump mass data are even more affected by selection effects. The slope of the starless and protostellar CMDs are very different for the two algorithms. Furthermore, the lack of high-mass starless cores, previously observed by H07 and implied by the shallow prestellar mass function found by Enoch et al. (2008) is not apparent in the GAUSSCLUMPS data. This would imply that either the shortage is not real or GAUSSCLUMPS does not allocate enough flux to high-mass clumps. Indeed, protostars which have more irregular, disrupted envelopes due to e.g. outflows are perhaps worse affected by the regular profiles used by GAUSSCLUMPS. This would cause a lack of high-mass protostellar clumps, which might explain the GAUSSCLUMPS results.

Fundamentally, we can never know the real population of clumps underlying any dataset. However, certain evolutionary trends *must* be present in any clump decomposition for it to be a believable representation of this true population. One clear example of this is the evolution of core size over time. Every simple model of collapse naturally has cores decreasing in size with time. This trend is *not* apparent for the CLFIND clumps. In addition, particular CLFIND clumps incorporate material that seems equally likely to go on to form part of their final mass or that of their neighbours. There-



fore, treating the properties of a CLFIND clump as representative of gravitationally-bound material in a single core is probably highly misleading. Of course, we may need to tweak the CLFIND parameters, increasing the lowest contour level and decreasing the contour separation, but any method which necessarily prevents overlap in a highly-cluster region, such as Perseus, will struggle to find the true source population. Since one is normally interested in the material that will go on to form the final star, GAUSSCLUMPS would seem the more representative algorithm choice.

Analysing the clumps found by two of the most popular clump-finding routines side-by-side, underlines the caution that one must exercise when comparing results from distinct studies on similar datasets in the *same* region. Different methods can produce very different results from the same data, providing clump populations that are not directly comparable. Future continuum and molecular-line surveys will need to carefully design their source extraction procedures to ensure objects are found at the desired length-scale without simply using an automated algorithm blindly.

## 7 ACKNOWLEDGMENTS

EIC thanks the Science and Technology Facilities Council (STFC) for studentship support while carrying out this work. The authors thank Jane Buckle and Gary Fuller for carefully reading and suggesting improvements to earlier versions of this paper and the referee, Derek Ward-Thompson, for his helpful suggestions that significantly improved the final version. The JCMT is operated by The Joint Astronomy Centre (JAC) on behalf of the STFC of the United Kingdom, the Netherlands Organisation for Scientific Research and the National Research Council (NRC) of Canada. We acknowledge the data analysis facilities provided by the Starlink Project which is maintained by JAC with support from STFC. This research used the facilities of the Canadian Astronomy Data Centre operated by the NRC with the support of the Canadian Space Agency.

## REFERENCES

Alves J., Lombardi M., Lada C. J., 2007, *A&A*, 462, L17  
 André P., Basu S., Inutsuka S., 2009, in Chabrier G., ed., *Structure Formation in Astrophysics*. Cambridge Univ. Press, Cambridge, p. 254  
 André P., Belloche A., Motte F., Peretto N., 2007, *A&A*, 472, 519  
 André P., Saraceno P., 2005, in Wilson A., ed., *Proc. Dusty and Molecular Universe: A Prelude to Herschel and ALMA*. Noordwijk, Netherlands: ESA Publ., p. 179  
 André P., Ward-Thompson D., Barsony M., 1993, *ApJ*, 406, 122  
 Ballesteros-Paredes J., Mac Low M.-M., 2002, *ApJ*, 570, 734  
 Basu S., Ciolek G. E., 2004, *ApJ*, 607, L39  
 Bate M. R., Bonnell I. A., 2005, *MNRAS*, 356, 1201  
 Berry D. S., Reinhold K., Jenness T., Economou F., 2007, in Shaw R. A., Hill F., Bell D. J., eds, *ASP Conf. Ser. Vol. 376, Astronomical Data Analysis Software and Systems XVI*. Astron. Soc. Pac., San Francisco, p. 425  
 Blitz L., 1993, in Levy E. H., Lunine J. I., eds, *Protostars and Planets III*. Univ. Arizona Press, Tucson, p. 125  
 Blitz L., Shu F. H., 1980, *ApJ*, 238, 148

Chabrier G., 2005, in Corbelli E., Palla F., Zinnecker H., eds, *The Initial Mass Function 50 Years Later*, *Astrophys. Space Sci. Library* Vol. 327. Springer, Dordrecht, p. 41  
 Ciolek G. E., Basu S., 2006, *ApJ*, 652, 442  
 Clark P. C., Klessen R. S., Bonnell I. A., 2007, *MNRAS*, 379, 57  
 Curtis E. I., Richer J. S., Buckle J. V., 2009, *MNRAS*, in press  
 Elmegreen B. G., Falgarone E., 1996, *ApJ*, 471, 816  
 Elmegreen B. G., Scalco J., 2004, *ARA&A*, 42, 211  
 Enoch M. L., et al., 2006, *ApJ*, 638, 293  
 Enoch M. L., Evans II N. J., Sargent A. I., Glenn J., Rosolowsky E., Myers P., 2008, *ApJ*, 684, 1240  
 Gammie C. F., Lin Y.-T., Stone J. M., Ostriker E. C., 2003, *ApJ*, 592, 203  
 Goodwin S. P., Kroupa P., Goodman A., Burkert A., 2007, in Reipurth B., Jewitt D., Keil K., eds, *Protostars and Planets V*. Univ. Arizona Press, Tucson, p. 133  
 Goodwin S. P., Nutter D., Kroupa P., Ward-Thompson D., Whitworth A. P., 2008, *A&A*, 477, 823  
 Goodwin S. P., Ward-Thompson D., Whitworth A. P., 2002, *MNRAS*, 330, 769  
 Hatchell J., Fuller G. A., 2008, *A&A*, 482, 855  
 Hatchell J., Fuller G. A., Richer J. S., Harries T. J., Ladd E. F., 2007, *A&A*, 468, 1009 (H07)  
 Hatchell J., Richer J. S., Fuller G. A., Qualtrough C. J., Ladd E. F., Chandler C. J., 2005, *A&A*, 440, 151  
 Heyer M., Krawczyk C., Duval J., Jackson J. M., 2009, *ApJ*, 699, 1092  
 Jijina J., Myers P. C., Adams F. C., 1999, *ApJS*, 125, 161  
 Johnstone D., Wilson C. D., Moriarty-Schieven G., Joncas G., Smith G., Gregersen E., Fich M., 2000, *ApJ*, 545, 327  
 Jones C. E., Basu S., Dubinski J., 2001, *ApJ*, 551, 387  
 Kirk H., Johnstone D., Di Francesco J., 2006, *ApJ*, 646, 1009  
 Kirk J. M., Ward-Thompson D., André P., 2005, *MNRAS*, 360, 1506  
 Klessen R. S., Burkert A., 2000, *ApJS*, 128, 287  
 Kroupa P., 2001, *MNRAS*, 322, 231  
 Lada C. J., Lada E. A., 2003, *ARA&A*, 41, 57  
 Li P. S., Norman M. L., Mac Low M.-M., Heitsch F., 2004, *ApJ*, 605, 800  
 Motte F., André P., Neri R., 1998, *A&A*, 336, 150  
 Myers P. C., Benson P. J., 1983, *ApJ*, 266, 309  
 Myers P. C., Fuller G. A., Goodman A. A., Benson P. J., 1991, *ApJ*, 376, 561  
 Nutter D., Ward-Thompson D., 2007, *MNRAS*, 374, 1413  
 Ossenkopf V., Henning T., 1994, *A&A*, 291, 943  
 Padoan P., Nordlund Å., 2002, *ApJ*, 576, 870  
 Reid M. A., Wilson C. D., 2006, *ApJ*, 650, 970  
 Rosolowsky E. W., Pineda J. E., Foster J. B., Borkin M. A., Kauffmann J., Caselli P., Myers P. C., Goodman A. A., 2008, *ApJS*, 175, 509  
 Salpeter E. E., 1955, *ApJ*, 121, 161  
 Scalco J., 2005, in Corbelli E., Palla F., Zinnecker H., eds, *The Initial Mass Function 50 Years Later*, *Astrophys. Space Sci. Library* Vol. 327. Springer, Dordrecht, p. 23  
 Schnee S., Li J., Goodman A. A., Sargent A. I., 2008, *ApJ*, 684, 1228  
 Schneider N., Brooks K., 2004, *Publ. Astron. Soc. Australia*, 21, 290  
 Shirley Y. L., Evans II N. J., Rawlings J. M. C., 2002, *ApJ*, 575,

337

- Simpson R. J., Nutter D., Ward-Thompson D., 2008, MNRAS, 391, 205
- Smith R. J., Clark P. C., Bonnell I. A., 2008, MNRAS, 391, 1091
- Solomon P. M., Rivolo A. R., Barrett J., Yahil A., 1987, ApJ, 319, 730
- Stutzki J., Bensch F., Heithausen A., Ossenkopf V., Zielinsky M., 1998, A&A, 336, 697
- Stutzki J., Güsten R., 1990, ApJ, 356, 513
- Swift J. J., Williams J. P., 2008, ApJ, 679, 552
- Tassis K., 2007, MNRAS, 379, L50
- Tassis K., Dowell C. D., Hildebrand R. H., Kirby L., Vaillancourt J. E., 2009, MNRAS, in press
- Ward-Thompson D., Scott P. F., Hills R. E., André P., 1994, MNRAS, 268, 276
- Ward-Thompson D., André P., Crutcher R., Johnstone D., Onishi T., Wilson C., 2007a, in Reipurth B., Jewitt D., Keil K., eds, Protostars and Planets V. Univ. Arizona Press, Tucson, p. 33
- Ward-Thompson D., et al., 2007b, PASP, 119, 855
- Williams J. P., Blitz L., McKee C. F., 2000, in Mannings V., Boss A. P., Russell S. S., eds, Protostars and Planets IV. Univ. Arizona Press, Tucson, p. 97
- Williams J. P., de Geus E. J., Blitz L., 1994, ApJ, 428, 693
- Young C. H., Shirley Y. L., Evans II N. J., Rawlings J. M. C., 2003, ApJS, 145, 111
- Zel'Dovich Y. B., 1970, A&A, 5, 84

## APPENDIX A: CLUMP CATALOGUES

This paper has been typeset from a  $\text{\TeX}/\text{\LaTeX}$  file prepared by the author.

**Table A1.** Properties of SCUBA clumps found with CLFIND. The full version of this table is available as Supplementary Material to the online version of this article.

Sub-region	Clump ID	RA <sup>a</sup> (J2000.0)	Dec <sup>a</sup> (J2000.0)	$R_{\text{eff}}$ <sup>b</sup> (pc)	$S_{\text{peak}}$ <sup>c</sup> (Jy beam <sup>-1</sup> )	$S_{850}$ <sup>d</sup> (Jy)	$M_{850}$ <sup>e</sup> ( $M_{\odot}$ )
NGC 1333	1	03:29:11.88	+31:13:09.4	0.020	3.47	17.56	21.02
NGC 1333	2	03:29:03.23	+31:15:57.5	0.030	3.34	22.23	26.61
NGC 1333	3	03:28:55.27	+31:14:36.5	0.043	2.76	21.71	25.98
NGC 1333	4	03:29:10.01	+31:13:39.4	0.024	2.18	10.71	12.82
NGC 1333	5	03:29:01.36	+31:20:30.5	0.052	1.40	23.48	28.11
...							

<sup>a</sup> Peak clump flux position.

<sup>b</sup> Clump effective radius, the geometric mean of the clump major and minor 'sizes' ( $\sqrt{\text{Size1} \times \text{Size2}}$ ). Each size is formed from the standard deviation of the clump co-ordinates about the centroid position, weighted by the pixel data values.

<sup>c</sup> Clump peak flux.

<sup>d</sup> Clump total flux.

<sup>e</sup> Clump mass derived from the total flux assuming optically thin, isothermal dust at 12 K (see section 3.3).

**Table A2.** Properties of SCUBA clumps found with GAUSSCLUMPS. The full version of this table is available as Supplementary Material to the online version of this article.

Sub-region	Clump ID	RA <sup>a</sup> (J2000.0)	Dec <sup>a</sup> (J2000.0)	$R_{\text{eff}}$ <sup>b</sup> (pc)	$S_{\text{peak}}$ <sup>c</sup> (Jy beam <sup>-1</sup> )	$S_{850}$ <sup>d</sup> (Jy)	$M_{850}$ <sup>e</sup> ( $M_{\odot}$ )
NGC 1333	1	03:29:11.41	+31:13:21.4	0.021	3.29	18.87	22.58
NGC 1333	2	03:29:02.99	+31:15:54.5	0.017	3.15	12.25	14.66
NGC 1333	3	03:28:55.27	+31:14:36.5	0.013	2.63	6.82	8.16
NGC 1333	4	03:29:01.36	+31:20:33.5	0.021	1.32	9.40	11.25
NGC 1333	5	03:29:11.19	+31:18:27.4	0.016	1.18	4.87	5.83
...							

<sup>a</sup> Peak clump flux position.

<sup>b</sup> Clump effective radius, the geometric mean of the clump major and minor 'sizes' ( $\sqrt{\text{Size1} \times \text{Size2}}$ ). Each size is formed from the standard deviation of the clump co-ordinates about the centroid position, weighted by the pixel data values.

<sup>c</sup> Clump peak flux.

<sup>d</sup> Clump total flux.

<sup>e</sup> Clump mass derived from the total flux assuming optically thin, isothermal dust at 12 K (see section 3.3).